Energy & Buildings 278 (2023) 112640

Contents lists available at ScienceDirect

Energy & Buildings

journal homepage: www.elsevier.com/locate/enb

Embodied carbon determination in the transportation stage of prefabricated constructions: A micro-level model using the bin-packing algorithm and modal analysis model

Yiming Xiang [a,*], Kehan Ma [a], Abdul-Majeed Mahamadu [a], Laura Florez-Perez [a], Ke Zhu [b], Yanhua Wu [c]

[a] Bartlett School of Sustainable Construction, University College London, London WC1E 7HB, UK
[b] School of Architecture, Southeast University, Sipailou Road, Nanjing 210096, China
[c] Architects & Engineers Co., Ltd. of Southeast University, Sipailou Road, Nanjing 210096, China

ARTICLE INFO

Article history:
Received 26 July 2022
Revised 22 October 2022
Accepted 3 November 2022
Available online 7 November 2022

Keywords:
Transportation carbon emissions
Prefabricated construction
Prefabricated elements
Bin packing
Modal model

ABSTRACT

The prefabricated construction generates considerable embodied carbon emissions during the manufacture, transportation, and construction stages. However, the contribution from the transportation stage is usually overlooked, leading to biases in life-cycle sustainability analysis of these projects. This article provides a micro-level transportation CE calculation method that estimates the project-specific emissions according to the features of prefabricated elements. The method simulates the transportation status of prefabricated elements as bin packing (BP) problems. Then, a modal analysis model is employed to calculate the CE of each vehicle based on vehicle type, road condition, and freight weight. Considering the minimum transportation CE as objective, a genetic algorithm is then used to search for the optimal solution and corresponding CE values. The comparative results among different CE calculation methods show that this BP-algorithm-based method provides reliable data across different loading rates, rendering the method suitable for calculating the transportation CE of prefabricated construction projects. Additionally, the BP-algorithm-based method differs the emission characteristics among different element types—the prefabricated floor generates the highest emissions, followed by prefabricated beam, wall, and column—suggesting the need to identify disparate emission factors for different element types and considering the sustainability aspects when selecting prefabricated approaches of projects. The results also highlight the efficiency of considering more prefabricated elements in a single transportation batch and selecting suitable vehicles for the optimisation of embodied carbon emissions. Architects, engineers, and contractors can use the method for project-specific transportation CE calculations and transportation planning. The calculation variables concerning the geometric features of prefabricated elements and vehicles can be adopted in the optimisation of project design and construction management for achieving less embodied carbon.

1. Introduction

Global carbon emissions (CE) reached 32 billion tons in 2020 [1]. As the main contributor, the construction industry consumes 36 % of global energy and produces 37 % of energy-related CO_2 emissions [2]. Apart from consuming operational energy for air-conditioning, heating, lighting, and operations of building equipment, buildings demand an inevitable supply of embodied energy through various products and processes used in initial construction, life-cycle maintenance, and final demolition [3]. In the future, the average percentage of embodied energy in the life-cycle energy of a building is predicted to rise as high as 60 % [4]. Therefore, the opportunity for energy reduction in embodied energy should not be ignored [5].

As a response, prefabrication is being increasingly adopted worldwide to alleviate the adverse environmental effects because the method has the potential to reduce the initial construction CE by 15 % compared to conventional methods [6]. *Prefabrication* is defined as a construction method where buildings are assembled with prefabricated elements [7]. As a result of manufacturing building elements in a specialised facility, the associated prefabrication process reduces material consumption in the construction process [8]. This reduction is believed to significantly contribute toward sustainability when adopting this modern construction method [6,9–12]. However, Teng *et al.* [13] challenged the asser-

* Corresponding author.
E-mail address: yiming.xiang.20@ucl.ac.uk (Y. Xiang).

https://doi.org/10.1016/j.enbuild.2022.112640
0378-7788/

Nomenclature

$area$	The windward area of the vehicle (m^2)
B	The set of boxes
B'	The set of residual boxes (boxes that are not placed)
b_i	The i-th box in set B
$b_i\prime$	A parameter set that defines each box b_i in the box set B
box_num_i	The selected sequence number of box in set B'
C	The set of containers
C_{i-j}	The j-th container of the i-the vehicle
CE_{3D-RSO}	The CE of 3D-RSO algorithm (kg CO_2e)
$CE_{benchmark}$	The benchmarked CE value (kg CO_2e)
$CE_{elements}$	The carbon emissions generated by moving only prefabricated elements to the construction site (kg CO_2e)
CE_{GA}	The CE of GA-based algorithm (kg CO_2e)
$CE_{vehicles}$	The carbon emissions generated by moving vehicles without freight to the construction site (kg CO_2e)
$CE(F)$	The CE of fleet F (kg CO_2e)
Coe_i	The CE coefficient of the transport method [kg CO_2e/(ton · km)]
Dis_i	The transport distance (km)
F	The set of vehicles
f_0	The emission rate of the vehicle operating with the STP value of 0 (kg CO_2e/h)
f_j	The CE rate of operating mode j (ton/h)
f_{scale}	The fixed mass of the vehicle (ton)
Fac_i	The CE factor of the transport method i (kg CO_2e/km)
G	A set of discrete variables that determines the selection between two space generation method in each placing
g	The acceleration due to gravity (9.8 m/s^2)
G_i	The selection of place generation method in the i-th time box placing
H_i	The height of S_i (m)
H_{i-j}	The height of C_{i-j} (m)
h_i	The height of b_i (m)
h_{i-1}	The extension length of the rebar on one of the height sides (m)
h_{i-2}	The height of precast concrete (m)
h_{i-3}	The extension length of the rebar on the other height side (m)
h_{i-4}	The interval between adjacent elements in the height dimension (m)
k_f	The coefficient factor of STP and emission rate (1000· kg^2 CO_2e/kWh)
L_i	The length of S_i (m)
L_{i-j}	The length of C_{i-j} (m)
l_i	The length of b_i (m)
l_{i-1}	The extension length of the rebar on one of the length sides (m)
l_{i-2}	The length of precast concrete (m)
l_{i-3}	The extension length of the rebar on the other length side (m)
l_{i-4}	The interval between adjacent elements in the length dimension (m)
$Layer_i$	The layer number of S_i
$length(B')$	The number of items in set B'
$length(S\prime)$	The number of items in set $S\prime$
$Load_{average}$	The average load capacity (ton)
$Load_i$	The load capacity of S_i (ton)
$Load_{i-j}$	The load capacity of C_{i-j} (ton)
$Load\_rate_i$	The average loading rate
m	Number of boxes in set F
m_{3D-RSO}	The number of vehicles of 3D-RSO algorithm
m_{GA}	The number of vehicles of GA-based algorithm
M_i	A discrete variable that represents the box placing method when S_i is used to place a box
Mal_i	The material quantity that transported by method i (ton)
$mass$	The total mass of individual vehicle (ton)
N	A set of float-type variables that determines the order of boxes O
n	Number of boxes in set B
O	The order of boxes to be packed
OMF_{i-j}	The fraction of time that V_i spent in the operating mode j
P	A set of float-type variables that determines the selection of a specific space in set $S\prime$ in each placing
p	The number of containers in V_i
P_i	A float-type variable that determine the selection of a specific space in set $S\prime$
r_{i-H}	The binary variable that determines whether b_i can rotate around the height (Z) axis. The value equals to 1 if the box can and 0 otherwise.
r_{i-L}	The binary variable that determines whether b_i can rotate around the length (X) axis. The value equals to 1 if the box can and 0 otherwise.
r_{i-W}	The binary variable that determines whether b_i can rotate around the width (Y) axis. The value equals to 1 if the box can and 0 otherwise.
res_{aero}	The aerodynamic drag coefficient (kW · sec^3/m^3)
res_{roll}	The rolling resistance coefficient (kW · sec/m)
res_{rotate}	The rotational resistance coefficient (kW · sec^2/m^2)
S	A sequence of parameter sets that defines each space in set of containers C
$S\prime$	The set of available space to place box b_i
S_i	The i-th space in the space set S
$space\_num_i$	the selected sequence number of space in set $S\prime$
$STP_{elements}$	The STP to move only prefabricated elements to the construction site (kW/ton)
STP_j	The STP of operating mode j (kW/ton)
STP_t	The STP at time t (kW/ton)
$STP_{vehicles}$	The STP to move vehicles without freight to the construction site (kW/ton)
T	A set of discrete variables that determines the selection among different vehicle types once a new vehicle is added
T_i	The type of i-th vehicle in the fleet F
$Time_i$	The operating hours of the i-th vehicle (V_i) in the fleet F (h)
$type\_num$	The total number of available vehicle types
V_i	The i-th vehicle in set F
v_t	The instantaneous vehicle velocity at time t (m/s)
v_num_i	The number of vehicles in which b_i is placed
W_i	The width of S_i (m)
w_i	The width of b_i (m)
w_{i-1}	The extension length of the rebar on one of the width sides (m)
w_{i-2}	The width of precast concrete (m)
w_{i-3}	The extension length of the rebar on the other width side (m)
w_{i-4}	The interval between adjacent elements in the width dimension (m)
W_{i-j}	The width of C_{i-j} (m)
$weight_i$	The weight of b_i (ton)
x_i	The X coordinate of the box b_i's bottom-left corner
y_i	The Y coordinate of the box b_i's bottom-left corner
z_i	The Z coordinate of the box b_i's bottom-left corner
α_t	The instantaneous vehicle acceleration (m/s^2)
θ_t	The road grade at time t
μ_{aero}	The aero drag coefficient of the vehicle
$\mu_{rolling}$	The rolling resistance coefficient of the vehicle (N/kN)

ρ_{aero}	The density of the air (1.29 kg/m^3)
$\rho_{material}$	The density of element material (ton/m^3)

Abbreviation

3D-RSO	Three-dimensional residual-space optimised algorithm
BP	Bin packing
CE	Carbon emissions
GA	Generic algorithm
STP	Scaled tractive power

tion that prefabrication can necessarily lead to reduced CE, particularly when the reusability of steel or wood structures is not considered.

This contradictory situation could be attributed to the neglections of some additional emissions in the conventional analysis of prefabrication construction, such as those caused by more severe transportation tasks and more complicated manufacturing processes. For instance, Sebaibi and Boutouil [14] reported that the construction elements produced in the prefabrication industry have a much higher environmental impact during manufacturing than elements produced by ready-mixed concrete due to specific thermal treatment processes during factory production. As a result, the disparity among different CE analysis models could achieve 50 % [10], suggesting that neglected CE are associated with some calculation methods.

The transportation CE of prefabrication is the worst-hit area of this problem with limited concerns [15]. Researchers commonly calculate transportation CE of prefabricated projects with averages or estimates based on assumptions without practical analysis [16], reporting a negligible and same-as-cast-in-situ transportation contribution [6,17] (1 %-8% of the total life-cycle CE [18]). However, a significant side effect of prefabrication is the decrease in transportation and hanging efficiency [19,20], which leads to more CE than conventional construction methods in these stages. Specifically, prefabricated elements occupy more space than the original materials, thus requiring more vehicles for handling and transport [15]. Meanwhile, the transportation through material supplier, offsite factory, and construction site increases the transportation distance, causing a 50 %-70 % increment in the transportation emissions and a 4 % CE increment during the construction process [21,22]. Considering prefabrication waste reduction reduces approximately 3 % of the total CE [9,22], the extra emissions caused by inefficient element transportation will, without effective management, offset or conceal environmental advantages during the manufacturing process.

CE calculation works as the precondition of sustainability analysis and optimisation. A reliable CE calculation method provides scholars with influence factors and their quantitative relationship to transportation CE, which can help identify effective optimisation solutions. By considering real-world transportation scenarios, the macro-level CE estimation can be detailed to a micro level, allowing for project-specific analysis and an objective comparison among design, construction, and transportation alternatives. The analysis of prefabrication construction will be distinguished from cast-in-situ construction, thus providing information on actual performance in real-world practices.

This article aims to calculate the transportation CE in the prefabricated construction process at the micro level. Specifically, the study employs the bin packing (BP) algorithm to simulate the transportation status of elements. By considering the prefabrication design codes and transportation limitations, the algorithm provides practical packing conditions according to different element sets (e.g., prefabricated columns, beams, etc.). A modal analysis model is then employed to calculate the transportation CE generated by each vehicle.

2. Literature review

2.1. Transportation carbon emissions

Transportation is essential in building delivery and generates non-negligible effects on the environmental impact of buildings. Excluding or ignoring transportation energy may cause a variation equal to 5 %-7% of the total life-cycle embodied energy [23]. This ratio may increase to more than 10 % when the prefabrication is adopted [11,22]. Mao *et al.* [9] identified the transportation phases in prefabrication construction as 1) transporting building materials from a distribution centre to the off-site prefabrication factory and from a distribution centre to the project site, 2) transporting prefabricated elements from off-site prefabrication factory to the project site, 3) transporting construction waste and soil from off-site prefabrication factory to landfill, or from project site to landfill, and 4) transporting construction equipment and workers. Among these four phases, phases 3 and 4 contribute to a limited percentage of the total life-cycle energy (both less than 1 %) [24]. Most research attention is thus drawn to the other two phases [18], especially the transportation of prefabricated elements that crucially affects the environmental benefits of prefabrication [9].

From the literature reviewed, there are two assumptions that impact the calculation and analysis on transportation CE: freight status and vehicle operation mode.

2.1.1. Freight status

In construction transportation analysis, freights have traditionally been considered as non-solid substances without fixed shapes. All vehicles are also assumed to reach an identical loading status and generate an average emissions value. Therefore, it is the material weight rather than size that dominates the transportation quantity in traditional transportation estimation. This assumption is widely used in the transportation CE calculation of cast-in-situ construction. For instance, Li *et al.* [25] calculated the transportation CE of a cast-in-situ residential building. The researchers considered the material weight, transport distance, and vehicle type (i.e., diesel-powered truck, electric locomotive) as variables and reported a 2 % total CE contribution of transportation. Similar calculation formulas were seen in the research of Jafary Nasab *et al.* [26], who analysed the carbon footprint in the construction phase of high rise construction in Tehran.

Abey and Anand [27] adopted the above assumption in their prefabrication transportation CE calculations and reported a similar transportation CE contribution between prefabrication and cast-in-situ construction (3 %-5%). Hao *et al.* [6] employed the same assumption and claimed that only 1 % CE is generated in the transportation stage of either prefabrication or cast-in-situ construction.

However, Wang *et al.* [15] claimed that the assumption (i.e., all vehicles achieve an identical loading rate) could not be directly applied to the CE calculation of prefabrication transportation because the actual loading rates of prefabricated elements vary based on the size limit, stacking layer limit, and installation sequence. For instance, prefabrication design codes set different maximum stacking layers for different prefabricated element types [28]. Real-world

constraints conflict with calculation assumptions and challenge the results of previous studies, especially at the project level.

Liu, Chen, *et al.* [29] and Liu, Yang, *et al.* [30] managed to overcome this defect using micro-level CE calculations. Both sets of researchers divided prefabricated elements into several branches according to the actual transportation plan. CE was calculated based on vehicles concerning specific load, distance, and transport approach. However, their system realises CE monitoring rather than prediction. Detailed results are also provided during or after the construction process. Meanwhile, the emission factors the researchers used were cited from Chen and Zhu [31], which is out-of-date and does not vary for different vehicle types and loading statuses.

2.1.2. Vehicle operation mode

In the studies mentioned in Section 2.1.1, vehicles were assumed to operate in controlled environments with idealised loading rate, stable speed, and temperate conditions. Therefore, average emission factors from macro-level statistics and laboratory measurements were adopted [15]. Yet these statistical data have significant variances from real-world emissions [32] due to the difference in driving cycles, vehicle technology, and emission regulations in different regions [33].

The modal model (e.g., *EMFAC*, *MOVES3*, and *HBEFA*) allows for calculations considering real-world driving status by providing specific emission factors for different 'operation modes', which are defined by internal observed (e.g., engine parameters) or externally observed (e.g., speed, acceleration, weight) variables [33]. For instance, *MOVES3* provides specific emission rates according to pollutant, emission process, fuel type, regulatory class, operating mode, and vehicle age [34]. Comparative studies between the modal model and statistical model (i.e., calculation using statistical data) show that the modal provides a more accurate emission estimation [35–37]. The modal model is, therefore, preferable in micro-level transportation CE analysis [33,38].

The development and application of the portable emission measurement system (PEMS) provide the emission characteristics of vehicles on actual roads, thus bringing the assumption of vehicle operation closer to reality [39]. Scholars have used actual measured data to identify the real-world emission characteristics of light-duty vehicles [40], heavy-duty vehicles [39,41], and non-road mobile machines [32,42,43]. These characteristics allow scholars to verify and adjust the general modal model, as shown in studies conducted by Wang, Tu *et al.* [33] and Seo *et al.* [44]. However, the sample size of studies using PEMS generally remains limited (1–2), which could be unrepresentative. Such studies also focused on the general situation in the logistic industry rather than practices in the prefabricated construction context.

2.2. Bin packing problem

The *BP problem* refers to packing a set of items into a minimum number of bins so that the sum of the item sizes in each bin is no greater than the bin capacity [45]. The problem can be categorised into one-, two-, and three-dimensional conditions for different practical applications [46]. Specifically, one-dimensional BP problems have many applications to problems of data management, scheduling, and resource allocation [47]; two-dimensional BP problems are used to solve problems in the cutting of corrugated or decorated material (wood, glass, cloth industries), and the newspapers paging [48]; and three-dimensional BP problems are applied in cutting and loading contexts (e.g., cutting of foam rubber in arm-chair production, container and pallet loading, and packaging design) and scheduling problems [49,50].

The BP problem is known to be NP-hard, which means that the existence of an efficient (polynomial-time) algorithm is unlikely. Consequently, computation times are expected to grow exponentially as the problem size increases. This characteristic motivates the search for heuristic, or approximate, solutions to instances of the problem [47]. Generally, most algorithms are employed to find reasonable, feasible solutions in an acceptable timescale rather than to search for every possible solution or combination [51].

The solution for BP problems can technically be divided into two steps: 1) exploring the suitable method to place the item, and 2) searching for the optimum placing result. In the same way, the development of solution algorithms can be summarised as 1) developing more accurate placing algorithms and 2) introducing more efficient searching algorithms [52]. Considering the existing advance in computer science, which could provide approximate or even exact optimal solutions, a promising research direction is to apply the solutions in practical scenarios [52].

Regarding applying BP solutions in transportation, scholars focus on modelling and solving actual problems in the logistics industry. The BP solution was originally applied to optimise the transportation plan of variable-sized items. Specifically, the prototype problem is defined as packing a subset of given rectangular three-dimensional boxes into a given rectangular container for the smallest container number and thus the lowest transportation cost [53]. Subsequent studies added more constraints on the packing method to solve specific issues, such as the freight priority [54], weight balance [55], product order and destination [56], transportation route [57], and time window [58], pushing the BP solutions closer to reality.

2.3. Research gaps

The transportation of prefabricated elements crucially impacts the CE of projects. However, limited attention has focused on the CE calculation in the transportation stage. Existing studies roughly simulated the transportation process as transferring homogeneous non-solid material by a fleet of identical vehicles in a stable environment, which deviates from the real-world transportation situation. As a result, the CE calculation method using actual transportation conditions demands further exploration and, more so, for the prefabricated construction context. This pursuit can be divided into two requirements: 1) the simulation of transportation status and 2) the CE calculation based on specific situations. Studies on the BP problems and the modal CE analysis model separately fills these two requirements, but an integrated solution to the transportation CE calculation has not yet emerged.

Therefore, this study seeks to determine a pathway for calculating the transportation CE of prefabricated elements considering real-world constraints by integrating the BP algorithm and modal analysis model. The research provides a practical and reliable transportation CE calculation method for the sustainability analysis of prefabrication construction.

3. Methodology

The methodology employed in this study involves four steps: 1) model the transportation status of prefabricated elements as a classic three-dimensional BP problem, 2) calculate the transportation CE using the modal analysis model, 3) explore the solution to the BP problem, and 4) compare the results to other methods for validation. The research content related to each step is explained in detail below.

3.1. Bin packing problem design

3.1.1. Problem description

The transportation of prefabricated elements is considered a three-dimensional BP problem with guillotine constraints. Specifi-

cally, this problem involves packing a set of three-dimensional rectangular boxes orthogonally into rectangular containers while satisfying the requirement that the packing is guillotine cuttable (i.e., there exists a series of face parallel straight cuts that can recursively cut the container into pieces so that each piece contains a box and that no box has been intersected by a cut [59]). Compared with simple orthogonal three-dimensional BP problems (which are usually adopted onsite [15]), the guillotine constraints allow for moving the prefabricated elements from the top of vehicles, thus reducing the time and difficulty of loading or unloading [52].

In this problem, prefabricated elements are considered a set of rectangular boxes, each of which has seven parameters, as shown in Eqs. (1)–(6). These equations are represented based on precast concrete elements and can be applied to other volumetric or panelised prefabricated element types (e.g., timber elements and steel elements) by adjusting the corresponding values.

$$B = \{b_1, \cdots, b_i, \cdots, b_n\} \tag{1}$$

$$b_i = \{l_i, w_i, h_i, r_{i-L}, r_{i-W}, r_{i-H}, weight_i\} \tag{2}$$

$$l_i = l_{i-1} + l_{i-2} + l_{i-3} + l_{i-4} \tag{3}$$

$$w_i = w_{i-1} + w_{i-2} + w_{i-3} + w_{i-4} \tag{4}$$

$$h_i = h_{i-1} + h_{i-2} + h_{i-3} + h_{i-4} \tag{5}$$

$$weight_i = l_{i-2} \times w_{i-2} \times h_{i-2} \times \rho_{material} \tag{6}$$

where n is the number of boxes; B is the set of n boxes; b_i is the i-th box in the set; l_i, w_i, and h_i are the length, width, and height (m) of b_i, respectively; r_{i-L}, r_{i-W}, and r_{i-H} are binary variables that determine whether the box can be rotated around the length (X), width (Y), and height (Z) axes, respectively. The value equals 1 if the box can be rotated and 0 otherwise; $weight_i$ is the weight of b_i (ton); l_{i-1}, l_{i-3}, w_{i-1}, w_{i-3}, h_{i-1}, and h_{i-3} are the extension length of the rebar on each side (m), respectively; l_{i-2}, w_{i-2}, and h_{i-2} are the length, width, and height of precast concrete (m), respectively; l_{i-4}, w_{i-4}, and h_{i-4} are the interval between adjacent elements in each dimension (m); and $\rho_{material}$ is the density of element material (ton/m^3), which is set to 2.5 ton/m^3 in precast concrete elements. The weight of extended rebar is excluded in the calculation because their weight only contributes to a minor part of the prefabricated elements' weight, thus leading to the negligible variance of the result. Fig. 1 describes the variables mentioned above.

The transportation space of vehicles is considered a set of rectangular containers with four parameters, as shown in Eqs. (7)–(10).

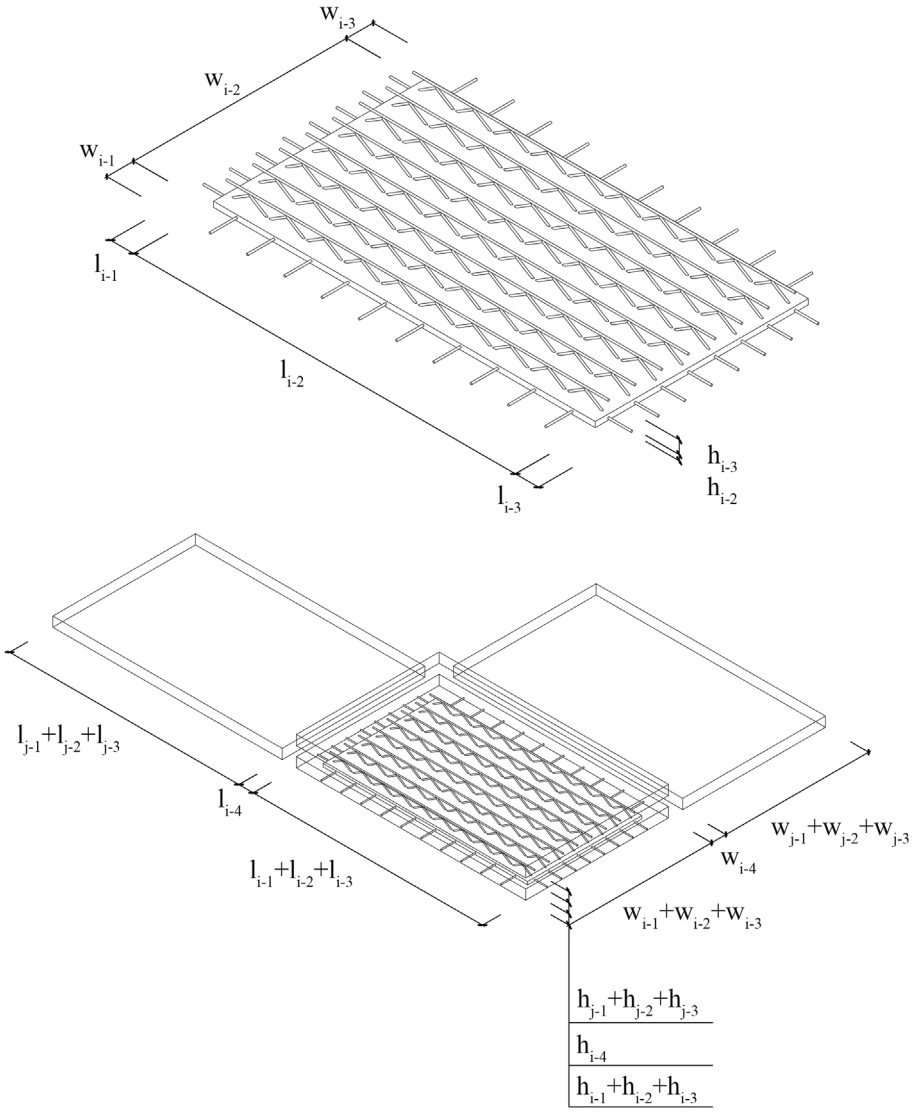

Fig. 1. Variables of the prototype prefabricated element.

$$F = \{V_1, \cdots, V_i, \cdots, V_m\} \tag{7}$$

$$V_i = \{C_{i-1}, \cdots, C_{i-j}, \cdots, C_p\} \tag{8}$$

$$C = \{C_{1-1}, \cdots, C_{i-j}, \cdots, C_{m-p}\} \tag{9}$$

$$C_{i-j} = \{L_{i-j}, W_{i-j}, H_{i-j}, Load_{i-j}\} \tag{10}$$

where m is the number of vehicles, F is the set of m vehicles in the transportation fleet; V_i is the i-th vehicle in F; C_{i-j} is the j-th container of the i-the vehicle; p is the number of containers in V_i; C is the set of containers; L_{i-j}, H_{i-j}, and W_{i-j} are length, width, and height of C_{i-j} (m), respectively; and $Load_{i-j}$ is the load capacity of C_{i-j} (ton).

The objective of the BP problem is to pack all the boxes in set B into a suitable container set C, thus minimising the total carbon emissions of fleet F. This aim is represented by Eq. (11) below:

$$min[CE(F)] \tag{11}$$

where $CE(F)$ is the CE of fleet F (kg CO_2e). The calculation method of CE is given in Section 3.2.

This packing problem has the following constraints:

C-1: All the boxes are packed orthogonally, i.e., every face of boxes is parallel to the faces of the containers.
C-2: The rotation of each box is strictly limited by the parameter of r_{i-X}, r_{i-Y}, and r_{i-Z}.
C-3: All the boxes are fully supported by either other boxes or the container, i.e., the bottom of each box is not allowed to hang in the air.
C-4: The packing is guillotine cuttable.
C-5: All the boxes must be packed.
C-6: Boxes are placed into containers without exceeding the length, width, height, and weight of each container.
C-7: The layer of packed boxes cannot exceed the limitation of corresponding codes (specific codes are cited in Section 4.2).

3.1.2. Variable determination

The packing of boxes is considered a recursion of a four-step process: 1) select a specific box, 2) select an available space to place the box, 3) place the box, and 4) update the available space. Correspondingly, the key to solve this problem is to determine 1) the order of boxes, 2) the available space, 3) the method to place the box, and 4) the update method of residual spaces.

The order of boxes O is determined by a set of float-type variables N, according to equations (12)-(16). These equations allow for determining the order of boxes without the limitation of box number, and the equations can therefore be used in a recursion process.

$$N = \{N_1, \cdots, N_i, \cdots, N_n\} \tag{12}$$

$$N_i \in [0, 1] \tag{13}$$

$$box\_num_i = N_i \times length(B') \tag{14}$$

$$B' \in B \tag{15}$$

$$O = \{box\_num_1, \cdots, box\_num_i, \cdots, box\_num_n\} \tag{16}$$

where B' is the set of residual boxes (boxes that are not placed); length B'is the number of items in B'and box_num_i represents the selected sequence number of box in B' (e.g., 5 means the fifth box in b'

The selection of available spaces is combined with the determination of the box placing method. Given a box bi, the set of available space to place box b_i is $S\prime$, and the selection of a specific space is determined by a float-type variable P_i. It works as shown in equations (17)-(19)

$$P_i \in [0, 1] \tag{17}$$

$$space\_num_i = P_i \times length(S\prime) \tag{18}$$

$$P = \{P_1, \cdots, P_i, \cdots, P_n\} \tag{19}$$

where $space\_num_i$ represents the selected sequence number of space in $S\prime$ (e.g., 5 means the fifth space in $S\prime$); $length(S\prime)$ is the number of items in $S\prime$; and P is the set of P_i. Regarding the placing method, the *bottom-up left-justified* method is employed (i.e., always placing the box at the lowest and the leftmost corner of a space) [60]. In this method, six placing alternatives exist, as shown in Fig. 2. Each alternative generates a corresponding available space

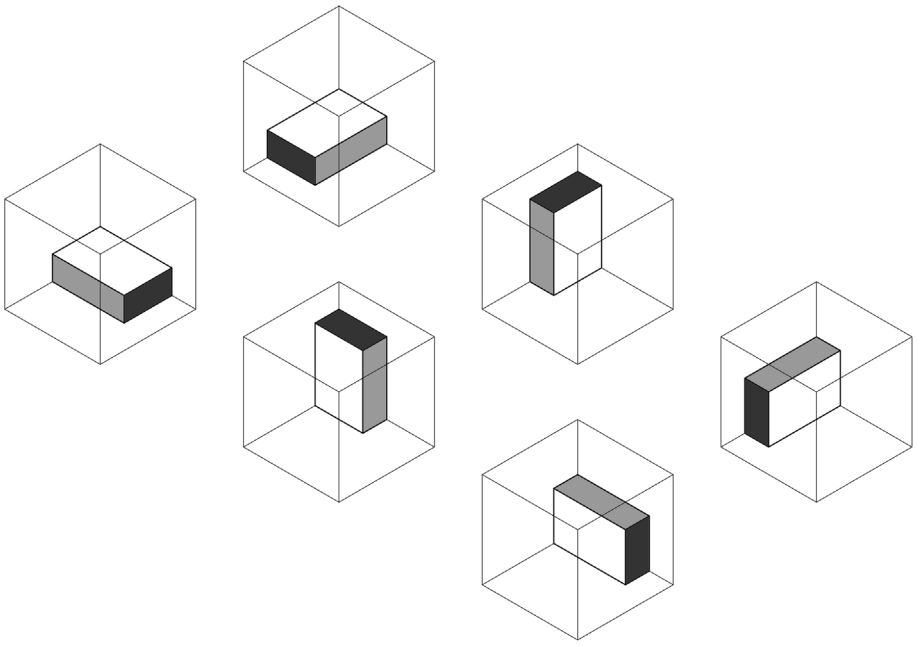

Fig. 2. Placing alternatives of boxes.

in the set of available space S. Thus, the selection among these six alternatives can also be represented by P_i.

A discrete variable set T determines the selection among different vehicle types once a new vehicle is added. It is calculated in Eqs. (20)–(22).

$$T = \{T_1, \cdots, T_i, \cdots, T_m\} \tag{20}$$

$$T_i \in \{1, 2, \cdots, type\_num\} \tag{21}$$

where T_i represents the type of i-th vehicle in the fleet F; and $type\_num$ is the total number of available vehicle types.

Concerning the update of residual space, once a box is placed, the selected space will be divided into several smaller and discrete sub-spaces in two ways due to the constraints of C-3 and C-4 (Fig. 3). The selection of these two methods is represented by a set of binary variables G, as shown in Eqs. (22)–(23).

$$G = \{G_1, \cdots, G_i, \cdots, G_n\} \tag{22}$$

$$G_i \in \{0, 1\} \tag{23}$$

where G_i represents the selection of the place generation method in the i-th time box placing.

Therefore, the objective of this algorithm is to search for the variable sets N, P, and G that have the lowest CE. Correspondingly, Eq. (11) can be transformed into the following equation to represent the objective of this bin packing problem:

$$min[CE(N, P, T, G)] \tag{24}$$

3.1.3. Algorithm development

The algorithm defined each box b_i in the box set B by a parameter set $b_{i\prime}$ as below:

$$b_{i\prime} = \{l_i, w_i, h_i, v\_num_i, x_i, y_i, z_i, r_{i-X}, r_{i-Y}, r_{i-Z}, weight_i\} \tag{25}$$

where v_num_i is the number of vehicles in which b_i is placed; and x_i, y_i, and z_i represent the coordinates of b_i's bottom-left corner.

The set of containers C is transformed to the set of spaces S, as defined in the equations (26)-(28), as below:

$$S = \{S_1, \cdots, S_i, \cdots, S_q\} \tag{26}$$

$$S_i = \{v\_num_i, L_i, W_i, H_i, X_i, Y_i, Z_i, Load_i, M_i, Layer_i\} \tag{27}$$

$$M_i \in \{0, 1, 2, 3, 4, 5\} \tag{28}$$

where q is the number of spaces; S_i is the i-th space in the space set S; L_i, W, and H_i are the length, width, and height (m) of S_i, respectively; $Load_i$ is the load capacity (ton) of S_i; M_i is a variable that represents the box placing method when S_i is used to place a box, as shown in Fig. 2; and $Layer_i$ is the layer number of S_i.

The pseudo-code of the BP algorithm is given as below:

For each box b_i in the box set B**:**
  define b_i by parameters as $b_{i\prime}$
  add b'_i to the residual box set $B\prime$
End
For *number* in the range [1, *length*(B)]**:**
  select a box b'_{number} in B' according to N_{number}
  While b'_{number} is not placed**:**
    For each space S_i in the space set S**:**
      If b'_{number} can be placed in S_i by the method of M**:**
        let $S_i(M_i) = M$
        add S_i to S'
      End
    End
    If S' is not an empty set**:**
      select a space S_{number} in S' according to P_{number}
      place b'_{number} in S_{number} according to $S_{number}(M_{number})$
      If the $S_{number}(Layer_{number})$ does not exceed the limitation**:**
        generate the new space S_{new} according to G_{number}
        add S_{new} to S
      End
      remove b'_{number} from B'
      identify b'_{number} as a placed box
    Else:
      vehicle_num += 1
      add a new vehicle and its corresponding space to S according to $T_{vehicle\_num}$
    End
  End
End

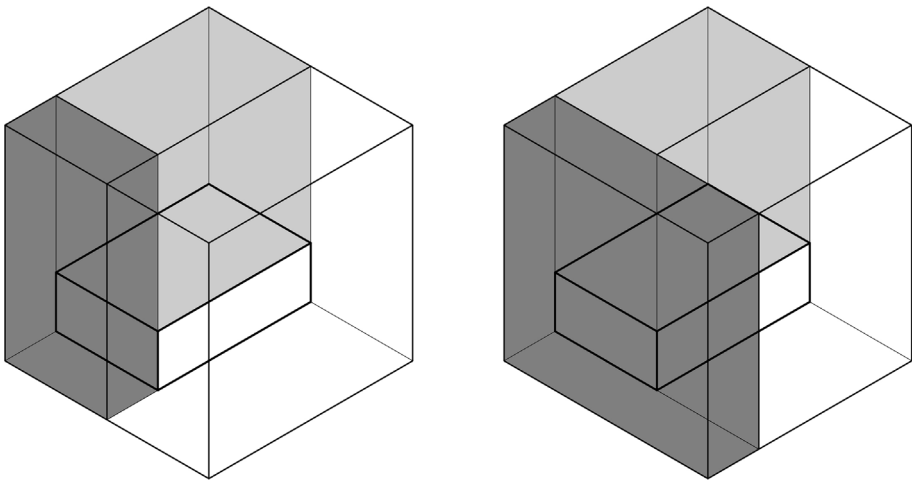

(a) (b)

Fig. 3. Space generation method whenG_i = 0 (a) andG_i = 1 (b).

3.2. Carbon emissions calculation

3.2.1. Calculation boundary

The research boundary of this article is the process of transporting the prefabricated elements from the factory to the construction site by vehicle. The emission process in this stage includes running exhaust, start exhaust, brake wear, tire wear, etc. [61]. Considering that running exhaust emissions (i.e., the archetypal mobile source emissions that generate during the operation of internal-combustion engines after the engine and emission control systems have stabilized at the specific operating temperature [61]) contribute to 98.85 % of CE [62], this study focuses only on emissions in this stage.

3.2.2. Data source

MOVES3 (*The United States Environmental Protection Agency's Motor Vehicle Emission Simulator*) is selected as the data source for the CE calculations in the case study of five Chinese projects (Section 4). It is a set of modelling tools for estimating air pollution emissions produced by on-road and nonroad mobile sources [62]. Although *MOVES3* is developed based on the emission data in California, USA, previous studies have reported the tool remains accurate in calculations outside California, especially in China [38,63]. Considering that the national modal emission model in China is rare [64], employing *MOVES3* for CE calculations is reasonable in this country.

3.2.3. Quantitative calculation

This study employs the calculation method for heavy-duty vehicles (with a gross vehicle weight rating of more than 8500 lbs) in the *Overview of EPA's Motor Vehicle Emission Simulator* [61]. The total running carbon emissions *CE* (kg CO_2e) of the fleet *F* is calculated by Eq. (29), as shown below:

$$CE = \sum \left[Time_i \times \sum \left(OMF_{i-j} \times f_j \right) \right] \tag{29}$$

where $Time_i$ is the operating hours of the *i*-th vehicle (V_i) in the fleet *F* (h); OMF_{i-j} is the fraction of time that V_i spent in the operating mode *j*; and f_j is the CE rate of operating mode *j* (ton/h).

MOVES3 classifies the CE rates of operating mode *f* using scaled tractive power (STP), as shown in Eqs. (30)–(34).

$$STP_t = \frac{res_{roll} v_t + res_{rotate} v_t^2 + res_{aero} v_t^3 + mass \times v_t(\alpha_t + g \times \sin\theta_t)}{f_{scale}} \tag{30}$$

$$res_{roll} = mass \times g \times \mu_{rolling} \times \cos\theta_t \tag{31}$$

$$res_{aero} = \frac{1}{2} \times \mu_{aero} \times \rho_{aero} \times area \tag{32}$$

$$mass_i = f_{scale\,i} + load_i \tag{33}$$

$$load_j = \sum_{b_i'(v_i=j)} b_i'(weight_i) \tag{34}$$

where STP_t is the STP at time *t* (kW/ton); res_{roll} is the rolling resistance coefficient (kW · *sec*/m); res_{rotate} is the rotational resistance coefficient (kW · sec^2/m^2); res_{aero} is the aerodynamic drag coefficient (kW · sec^3/m^3); *mass* is the total mass of the individual vehicle (ton); v_t is the instantaneous vehicle velocity at time *t* (m/s); α_t is the instantaneous vehicle acceleration (m/s^2); *g* is the acceleration due to gravity (9.8 m/s^2); θ_t is the road grade at time *t*; f_{scale} is the fixed mass of the vehicle (ton); $\mu_{rolling}$ is the rolling resistance coefficient of the vehicle (N/kN); μ_{aero} is the aero drag coefficient of the vehicle; ρ_{aero} is the density of the air (1.29 kg/m^3); and *area* is the windward area of the vehicle (m^2).

The carbon emission rate of operating mode *j* (f_j) is linearly related to the STP of the operating mode [62], and f_j can be calculated using Eq. (31).

$$f_j = k_f \times STP_j + f\_0 \tag{31}$$

where *STP_j* is the STP of operating mode *j* (kW/ton); *f_0* is the emission rate of the vehicle operating with the STP value of 0 (kg CO_2e/h); and k_f is the coefficient factor of STP and emission rate (1000· kg^2 CO_2e/kWh), which can be obtained through regression analysis on the emission data of *MOVES3*.

3.3. Exploration of solutions

This study employs a genetic algorithm (GA) to search for solutions to the bin packing problem defined in Section 3.1. The bin packing problem is first modelled in standard Python 3.8. Then, Geatpy 2.6.0—a genetic and evolutionary algorithm toolbox for Python [65]—is used to explore the result of Eq. (24).

3.4. Results validation

3.4.1. Validation of bin packing solutions

In the assumption that prefabricated elements are transported by identical vehicles on a straight road with stable features at a stable speed, and the freight does not change the windward area, Eq. (30) can be transformed as shown below:

$$STP_t = \frac{\left(mass \times g \times \mu_{rolling} \times \cos\theta_t + C v_t^2 + mass \times g \times \sin\theta_t \right) \times v_t}{f_{scale}} \tag{32}$$

$$= \frac{\left(\mu_{rolling} \times \cos\theta_t + \sin\theta_t \right) \times v_t g}{f_{scale}} load + \frac{\left(\mu_{rolling} \times \cos\theta_t + \sin\theta_t \right) \times v_t g}{f_{scale}} f_{scale} + \frac{C v_t^3}{f_{scale}} \tag{33}$$

$$= D \times load + E \tag{34}$$

where

$$D = \frac{\left(\mu_{rolling} \times \cos\theta_t + \sin\theta_t \right) \times v_t g}{f_{scale}} \tag{35}$$

$$E = \left(\mu_{rolling} \times \cos\theta_t + \sin\theta_t \right) \times v_t g + \frac{C v_t^3}{f_{scale}} \tag{36}$$

Accordingly, Eq. (29) can be rewritten as follows:

$$CE = \sum \left[Time_i \times f_i \right] \tag{37}$$

$$= Time_i \times \sum \left[k_f \times \left(STP_j - STP_{min} \right) + f\_min \right] \tag{38}$$

$$= Time_i \times \sum \left[k_f \times \left(D \times load + E - STP_{min} \right) + f\_min \right] \tag{39}$$

$$= Time_i \sum \left(k_f \times D \times load \right) + T_i \sum \left[f\_min + k_f (E - STP_{min}) \right] \tag{40}$$

$$= Time_i \times k_f \times D \times \sum load + \left[k_f (E - STP_{min}) + f\_min \right] \times Time_i \times m \tag{41}$$

Equations (34) and (41) can be re-interpreted as equations (42) and (43), respectively:

$$STP = STP_{elements} + STP_{vehicles} \tag{42}$$

$$CE = CE_{elements} + CE_{vehicles} \tag{43}$$

where $STP_{elements}$ is the STP to move only prefabricated elements to the construction site (kW/ton); $STP_{vehicles}$ is the STP to move vehicles without freight to the construction site (kW/ton); $CE_{elements}$ is the CE generated by moving only prefabricated elements to the construction site (kg CO_2e); and $CE_{vehicles}$ is the carbon emissions generated by moving vehicles without freight to the construction site (kg CO_2e).

As the total weight of prefabricated elements is a fixed value, the objective defined by Eq. (22) can then be transformed as

$$\min(m) \tag{44}$$

The objective defined by Eq. (44) is the same as the aim of classical bin packing problems, and thus it can be solved using classical bin packing algorithms. This study adopts the results of the *three-dimensional residual-space optimised algorithm (3D-RSO)* [52] as the benchmark. The pseudo-code of this algorithm is given below:

For each box b_i in the box set B**:**
  define b_i by parameters as b_i'
  add b_i' to the residual box set $B\prime$
End
sort B' in descending order according to the maximum possible bottom area of each box
While B' is not an empty set**:**
  select the first box b_1' in B'
  For each space S_i in the space set S**:**
    If b_1' can be placed in S_i by a method**:**
      calculate the performance of residual space after placing b_1' by this method
      add S_i to S'
    End
  End
  If S ′ is not an empty set**:**
    sort S ′ in descending order according to the performance of residual space
    select the first space S_1' in S'
    place b_1' in S_1' according to the corresponding method
    generate new space S_{new} with the largest residual space
    add S_{new} to S
    remove b_1' from B'
  Else:
    add a new vehicle and its corresponding space to S
  End
End

The 3D-RSO algorithm employs predefined formulas to determine the box order, box placing method, and generation method of new spaces after box placing, thus producing an acceptable result very quickly (less than 1 s). However, a global optimum of solutions can hardly be achieved without heuristic algorithms. Therefore, the criterion in bin packing solutions validation is that the results from the algorithm with GA (GA-based algorithm) should be equal to or better than the results of the 3D-RSO algorithm. This requirement is represented by the following equations:

$$m_{GA} \le m_{3D-RSO} \tag{45}$$

$$CE_{GA} \le CE_{3D-RSO} \tag{46}$$

where m_B and m_{3D-RSO} are the number of vehicles of GA-based algorithm and 3D-RSO algorithm, respectively; and CE_{GA} and CE_{3D-RSO} are the CE of GA-based algorithm and 3D-RSO algorithm (kg CO_2e), respectively.

3.4.2. Validation of CE calculation

The CE calculation is validated through conducting quantitative comparisons between the results of different calculation methods. The benchmarked calculation method and emission rate are selected from the *China Products Carbon Footprint Factors Database* [66,67] and the *Calculation Standard of Building Carbon Emissions GB/T51366-2019* [68]. The CE is calculated based on these two sources using the following equations:

$$CE_{benchmark} = \sum Mal_i \times Dis_i \times Coe_i \tag{47}$$

$$Coe_i = \frac{Fac_i}{Load_{average} \times Load\_rate_i} \tag{48}$$

where $CE_{benchmark}$ is the benchmarked CE value (kg CO_2e); Mal_i is the material quantity transported by method i (ton); Dis_i is the transport distance (km); Coe_i is the CE coefficient of the transport method [kg CO_2e/(ton · km)]; Fac_i is the CE factor of the transport method i (kg CO_2e/km); $Load_{average}$ is the average load capacity (ton); and $Load\_rate_i$ is the average loading rate.

4. Case study

4.1. Sample buildings

This article employs five real-built cases using the precast concrete structure to show the transportation carbon emissions calculation of prefabricated elements. The five buildings are all located in China: two residential buildings (Project A and B), one apartment building (Project C), one office building (Project D), and one education building (Project E), as shown in Fig. 4 and Table 1. Considered element types include prefabricated floor slab (floor), shear wall slab (wall), column, and beam.

Fig. 5 provides information on the geometric features of prefabricated elements in these five projects. In the figure, the x-axis represents the dimension of length (m) and the y-axis represents the dimension of width and height (m). Specifically, the l_i and w_i of each prefabricated element are shown by the x- and y-coordinates of a dot, respectively. The value of h_i is given by the height of a vertical bar (corresponding to the dot) at the bottom of each figure. Fig. 5 also shows the distribution of elements' size by colour transparency. A darker colour means a greater gathering of points and bars (i.e., more prefabricated elements are in such a specific size).

4.2. Data collection

The data collected in this study include 1) prefabricated element data, including the type, size, weight of elements used in the project; 2) CE data, including emission factor and application conditions adopted in either method; 3) vehicle data, including the type, size, load capacity, and resistance factor of vehicles; and 4) transportation data, including transportation constraints and road features.

The data of prefabricated elements are extracted from the design files (i.e., the design drawings and schedules). Content analysis is then conducted on those drawings to obtain the value of variables concerning l_i, w_i, h_i, and $weight_i$. The drawings of projects are examined and verified by all participants to ensure data quality.

This study employs CE data from *MOVES3*. Specific value set are selected according to the parameters of alternatives vehicles listed in Table 2. The table also includes the sources of vehicle and transportation data.

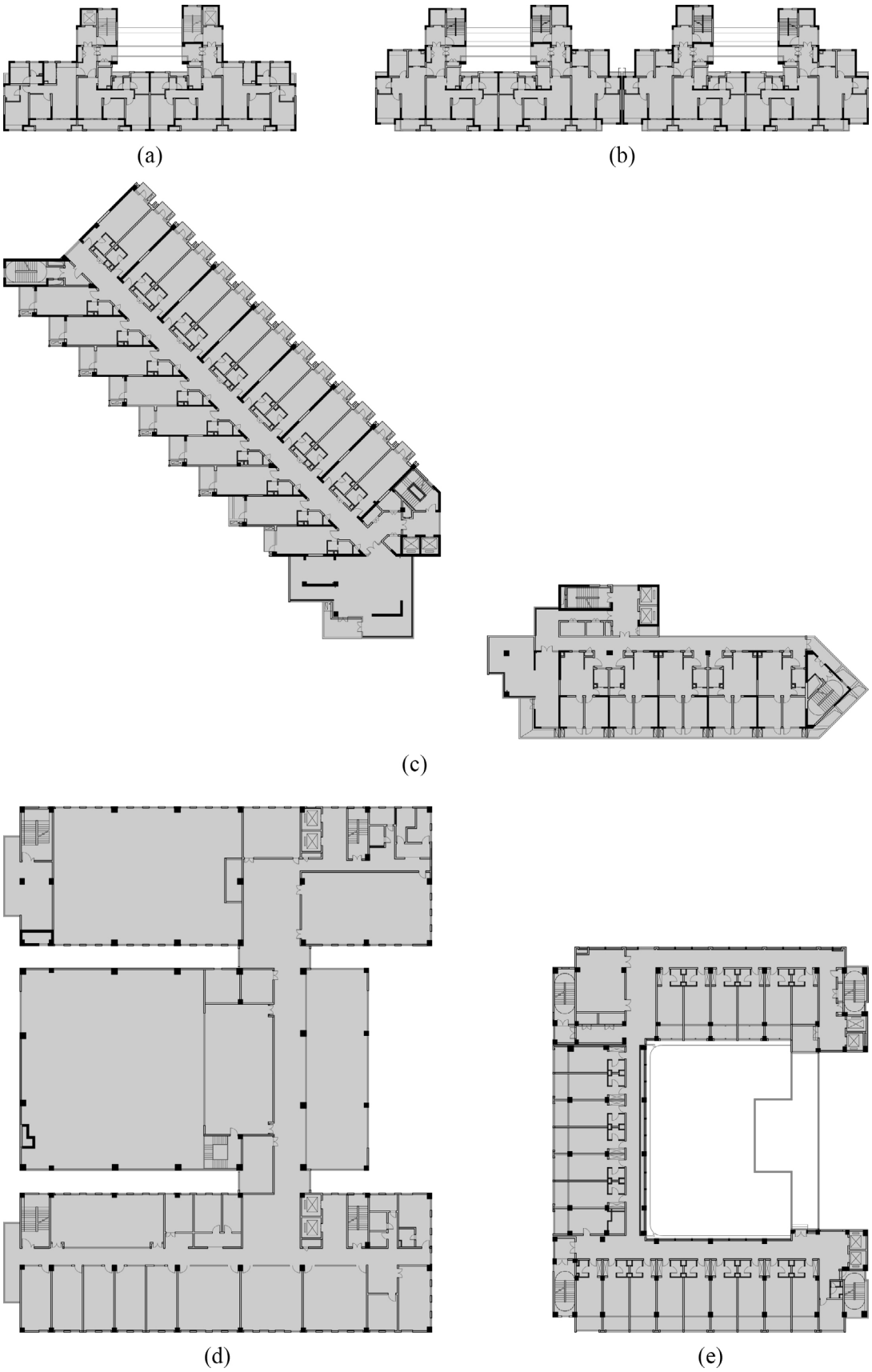

Fig. 4. Plan layout of Project A (a), B (b), C (c), D (d), and E (e).

Table 1
Summary of sample buildings.

Description	Project A	Project B	Project C	Project D	Project E
Types	Residence	Residence	Apartment	Office	School
Floor area (m^2)	454.79	751.54	2083.54	3298.96	1371.43
Layer number	20	18	17	6	6
Floor to floor height (m)	2.90	2.90	3.50	3.82	3.25
Element types, pieces, and weight (ton) per floor	Floor slab × 59 42.71 Shear wall slab × 10 17.26	Floor slab × 110 74.68 Shear wall slab × 20 32.36	Floor slab × 168 194.93 Shear wall slab x69 236.01 Column × 10 34.04 Beamx41 13.67	Floor slab × 155 219.08 Column × 20 65.42 Beam × 119 429.15	Floor slab × 90 89.59 Column × 44 104.79
Total weight of prefabricated elements per floor (ton)	59.97	107.04	478.65	713.65	194.38

4.3. Parameter settings

The transportation CE calculation is conducted based on the following conditions:

1) All the prefabricated elements are transported in Jiangsu Province, China, on a sector of the G40 road without the consideration of vehicle rotation.
2) All the vehicles are moving at a stable speed at 0 °C with standard atmospheric pressure.
3) All the prefabricated elements of a project are first divided by floors and then divided by their types into different batches (e.g., the floor batch of the first floor).
4) Elements in the same batch are packed by the off-line mode, i.e., all the elements are known before packing.

Considering the transportation code and current situation in China, this study set two vehicle alternatives. Vehicle 1 has a size of 13.75 m X 3 m X 4 m (Length X Width X Height) and a 15.3-ton self-weight. Vehicle 2 has a size of 17.5 m X 3 m X 4 m and a 16.8-ton self-weight. The upper limitation of the gross mass of these two vehicles are both 49 ton; thus, the load capacity of vehicles 1 and 2 are 33.7 ton and 33.2 ton, respectively. The transportation space of each vehicle is represented by two rectangular containers, as shown in Fig. 6.

Fig. 7 gives information on the packing status of different element types. All types of elements are packed horizontally and allow for rotation around one dimension. A detailed description of calculation parameters is provided in Table 2.

5. Results

5.1. Bin packing solutions

The GA-based BP algorithm generally shows better performance than the 3D-RSO algorithm in packing prefabricated elements of five sample buildings, as shown in Fig. 8. The number of vehicles employed by the GA-based algorithm is equal to or less than 3D-RSO algorithms using either vehicle 1 or 2, filling the demand of Eq. (45). Generally, the larger the total number of vehicles used, the larger the difference between those two algorithms.

Meanwhile, the 3D-RSO algorithm employs more vehicles, in most cases, when using vehicle 1 than vehicle 2. As shown in Table 2, vehicle 1 has a larger load capacity and a smaller space size than vehicle 2. Therefore, element size rather than element weight has a dominant effect on vehicle numbers in the transportation CE analysis on the sample buildings. Notably, the 3D-RSO algorithm using vehicle 1 in the transportation of prefabricated beams of Project D does not produce any data because the elements' size exceeds the dimensions of the available spaces in vehicle 1.

5.2. CE calculation

Fig. 9 compares the variation of transportation CE with loading rate among the BP method and two validation methods. Results show that the CE of these three methods are linearly related to the loading rate. In the analysis of vehicle 1, the slopes of the BP method, validation method 1 with Coe_i _1 (0.047), and validation method 2 with Coe_i _2 (0.059) are 20.02, 79.20, and 99.42, respectively. The interceptions of the three methods are 34.51, 0, and 0, respectively. The line of BP method is interpreted as following: when transporting prefabricated elements on a 50 km section on the G40 road by vehicle 1, the CE of driving an empty vehicle is 34.51 (kg CO_2e); for every 1 % increase in the loading rate (i.e., every 0.337-ton increase in the loading weight), the CE increases by 0.2002 (kg CO_2e). Similarly, lines of validation methods 1 and 2 mean the CE of driving an empty vehicle is 0 (kg CO_2e), and every 1 % increase in the loading rate will increase the CE by 0.7920 and 0.9942 (kg CO_2e), respectively. The same analysis can be applied in the case of vehicle 2, where the slopes of the BP method, validation method 1, and validation method 2 are 11.42, 75.67, and 94.99, respectively, and the interceptions are 33.26, 0, and 0, respectively.

The line of the BP method intersects with the lines of validation methods 1 and 2 at points around 57 % and 47 %, respectively. Considering a ± 10 % interval, the intersection range will be around 50 %-65 % (0.047) and 37 %-50 % (0.059), respectively. These ranges mean that the CE calculation result of the BP method is consistent with the result of the *China Products Carbon Footprint Factors Database* [66,67] and the *Calculation Standard of Building Carbon Emissions GB/T51366-2019* [68] when the average loading rate is at 50 %-65 % and 37 %-50 %, respectively. School of Transportation and Logistics of Southwest Jiaotong University [69] reported that the average loading rate of heavy-duty vehicles in Jiangsu province is between 40 % and 65 %, which indicates that the average carbon emissions factor Coe_i _1 (0.047) is very likely measured with a 0.40–0.65 loading rate ($Load\_rate_i$), which covers the intersection range of 50–65 %. Therefore, the calculation result of the BP method could very likely be close to the average real-world emissions. However, the average loading rate of building materials is between 69 % and 99 %, which is outside the intersection range of the BP method and Coe_i _2 (0.059). As a higher loading rate should lead to a lower carbon emission factor Coe_i, a greater loading rate (69 %-99 % vs 40 %-65 %) with a higher factor value (0.059 vs 0.047) suggests that the emission factor of 0.059 may not be consistent with the real-world emissions.

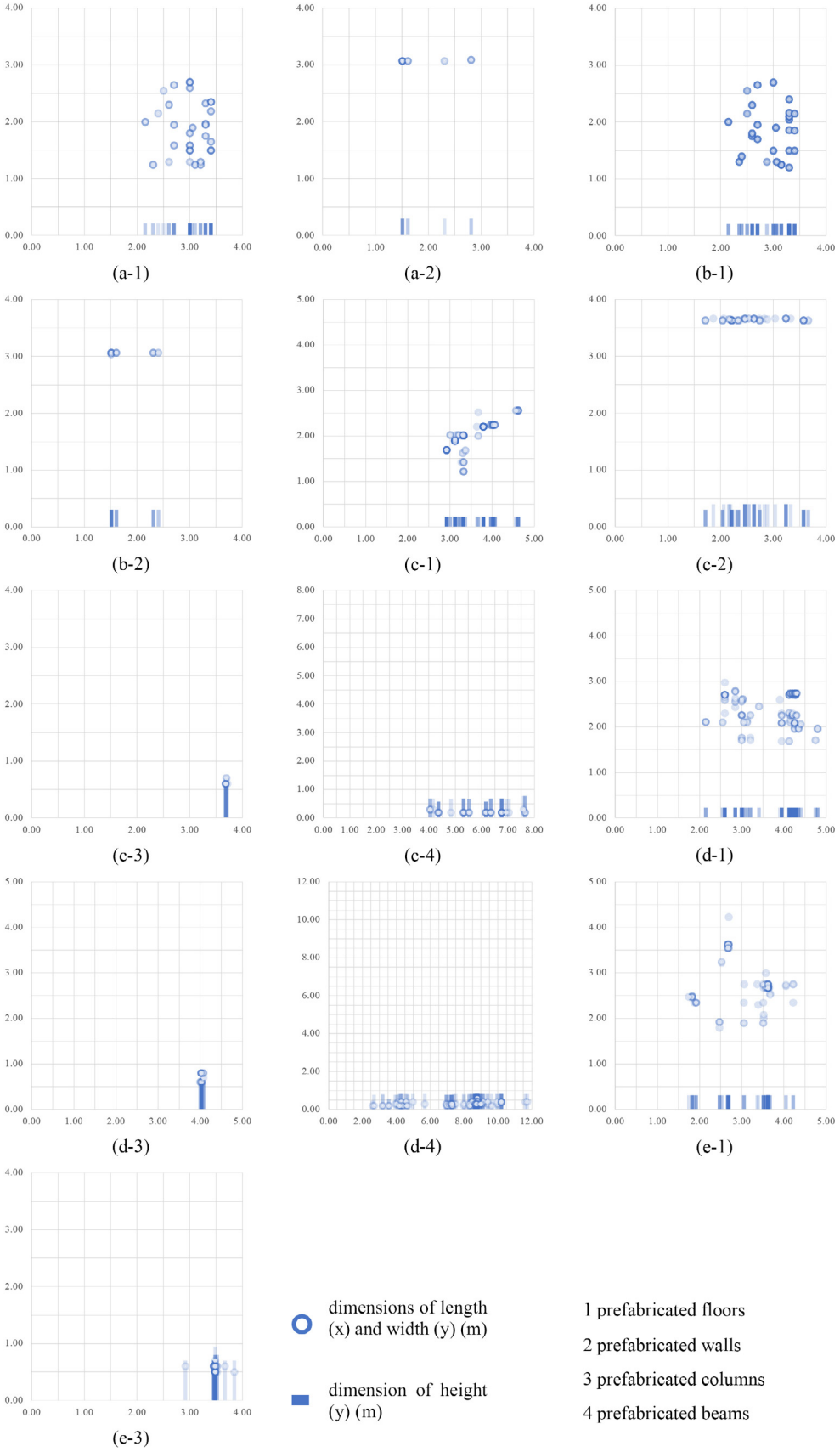

Fig. 5. Features of prefabricated elements in Project A (a), B (b), C (c), D (d), and E (e).

Table 2
Variable settings of the CE calculation.

Settings			Value	Data source
Vehicle				
Vehicle 1	Size	Length (m)	13.75	[69–71]
		Width (m)	3	
		Height (m)	4	
	Load	$Load_1$(ton)	33.7	
	Weight	f_{scale}(ton)	15.3	
	Resistance	$\mu_{rolling}$(N/kN)	6.8	
		μ_{aero}	0.75	
	Fuel		Diesel	
	Space			
	Space 1	Length (m)	4	
		Width (m)	3	
		Height (m)	2.4	
		$Load_{1\_1}$(ton)	33.7	
	Space 2	Length (m)	9.75	
		Width (m)	3	
		Height (m)	3	
		$Load_{1\_2}$(ton)	33.7	
Vehicle 2	Size	Length (m)	17.5	[69–71]
		Width (m)	3	
		Height (m)	4	
	Load	$Load_2$(ton)	32.2	
	Weight	f_{scale}(ton)	16.8	
	Resistance	$\mu_{rolling}$(N/kN)	6.8	
		μ_{aero}	0.75	
	Fuel		Diesel	
	Space			
	Space 1	Length (m)	4	
		Width (m)	3	
		Height (m)	2.4	
		$Load_{2\_1}$(ton)	32.2	
	Space 2	Length (m)	13.5	
		Width (m)	3	
		Height (m)	2.7	
		$Load_{2\_2}$(ton)	32.2	
Transportation				
Constraints	Floor	Stack mode	Horizontal	[28,72]
		$Layer_i$	≤ 6	
		r_{i_L}	0	
		r_{i_W}	0	
		r_{i_H}	1	
	Wall	Stack mode	Horizontal	
		$Layer_i$	≤ 6	
		r_{i_L}	0	
		r_{i_W}	0	
		r_{i_H}	1	
	Column	Stack mode	Horizontal	
		$Layer_i$	≤ 3	
		r_{i_L}	1	
		r_{i_W}	0	
		r_{i_H}	0	
	Beam	Stack mode	Horizontal	
		$Layer_i$	≤ 2	
		r_{i_L}	0	
		r_{i_W}	0	
		r_{i_H}	1	
Road	$\tan\theta_t$ and slope in percentage	−0.005	3.88 %	[73,74]
		−0.004	30.62 %	
		0.000	45.54 %	
		0.006	13.57 %	
		0.007	6.39 %	
	Distance	Distance (km)	50	
Speed	Speed	v_t(km/h)	59.08	[67]
Loading status	Loading rate	$Load\_rate_i$	0.40–0.65	[69]
CE calculation				
	BP method	k_f(1000 kg^2 CO_2e/kWh)	9.82×10^{-3}	[62]
		f_0(kg CO_2e/h)	13.57	
	Validation method 1	Coe_i _1 [kg CO_2e/(ton · km)]	0.047	[66,67]
	Validation method 2	Coe_i _2 [kg CO_2e/(ton · km)]	0.059	[68]

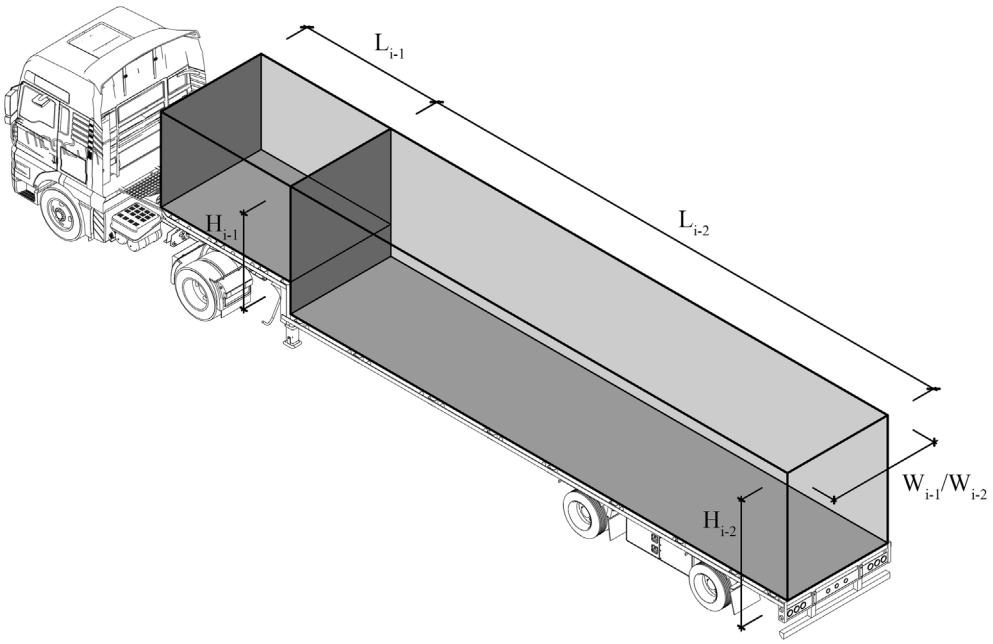

Fig. 6. Space division of the vehicle.

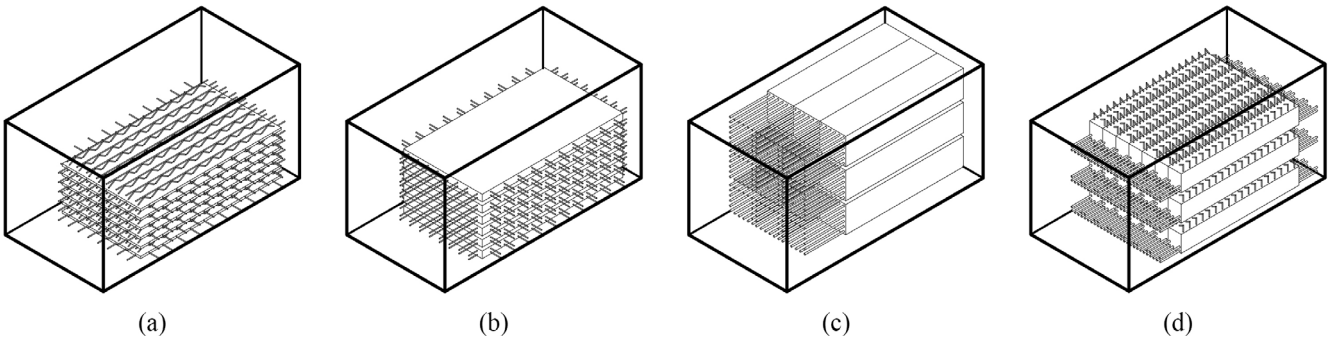

Fig. 7. Packing status of prefabricated floors (a), walls (b), columns (c), and beams (d).

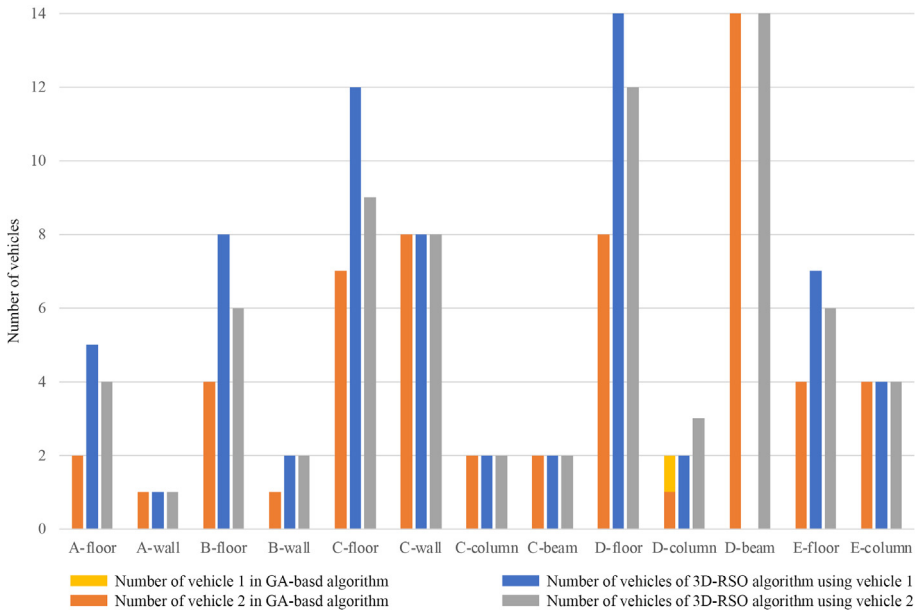

Fig. 8. Number of vehicles in GA-based BP algorithm and 3D-RSO algorithm.

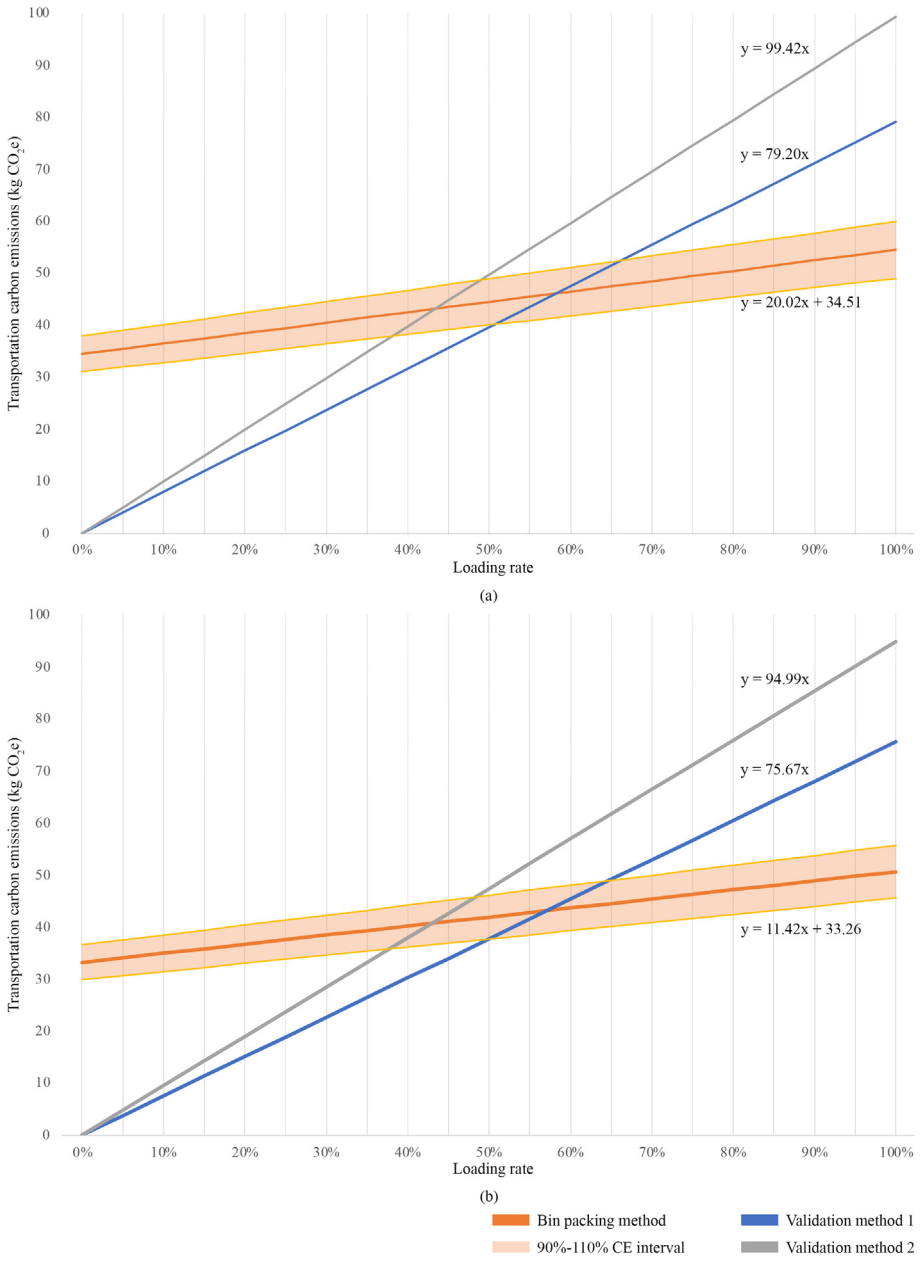

Fig. 9. CE variation with loading rate of vehicle 1 (a) and vehicle 2 (b).

5.3. Transportation CE of prefabricated elements

This study calculates the transportation CE of prefabricated elements in five projects (13 transportation tasks) using the GA-based BP algorithm, 3D-RSO algorithm using vehicle 1, 3D-RSO algorithm using vehicle 2, validation method 1 using the emission factor of 0.047 [kg CO_2e/(ton · km)], and validation method using the emission factor of 0.059 [kg CO_2e/(ton · km)], as shown in Table 3 and Fig. 10. The appendix files provide the detailed solutions for the GA-based BP algorithm and 3D-RSO algorithms.

Generally, the GA-based BP algorithm has the lowest CE compared to other methods. This result fulfils Eq. (46) so that the GA-based algorithm has a lower or equal CE to the 3D-RSO algorithm. The result also remains consistent with Section 5.1, underscoring that the GA-based method employs the least number of vehicles in the same situation comparing to other methods. However, no stable relationship exists between the results of 3D-RSO algorithms and validation methods 1 and 2.

As the total CE is mainly affected by the quantity of transported elements, it is more objective to compare the CE per unit of prefabricated elements. Therefore, Fig. 11 compares the average CE per unit weight of elements; the dotted lines of 2.35 and 2.95 are two benchmark values calculated using Coe_i _1 (0.047) and Coe_i _2 (0.059) (i.e., the CE of transporting one ton of prefabricated elements for 50 km), respectively. The CE values are categorised into four groups according to the element types: prefabricated floors, walls, columns, and beams. The GA-based algorithm provides the lowest CE in most tasks, except in the transportation of prefabricated walls in Project-A and prefabricated columns in Project-D, where the result (2.45 and 2.49) is minorly higher than the benchmark result of 2.35.

Regarding the result of 3D-RSO algorithms, when vehicle 1 is adopted, the CE is higher than 2.35 in all five transportation tasks of prefabricated floors and two of three wall transportation tasks. In contrast, results of this method are lower than 2.35 in two of three column transportation tasks and in both beam transportation

Table 3
Transportation CE of prefabricated elements in Projects A-E (kg CO_2e).

Project	Elements	GA-based algorithm	3D-RSO algorithm (vehicle 1)	3D-RSO algorithm (vehicle 2)	Validation method 1 (0.047)	Validation method 2 (0.059)
A	Floor	89.63	197.91	156.16	100.38	126.01
	Wall	42.67	44.83	42.67	40.85	51.29
B	Floor	173.45	320.42	239.98	175.50	220.31
	Wall	53.72	88.23	84.03	76.03	95.45
C	Floor	338.29	529.87	404.82	458.09	575.05
	Wall	393.77	409.83	393.77	554.62	696.23
	Column	84.94	88.01	84.94	79.97	100.39
	Beam	94.98	100.26	94.98	123.61	155.16
D	Floor	384.61	613.23	517.67	514.83	646.28
	Column	104.93	106.17	135.18	153.74	193.00
	Beam	697.82	–	697.82	1008.50	1265.99
E	Floor	181.51	290.93	248.04	210.53	264.28
	Column	189.73	197.26	189.73	246.25	309.12

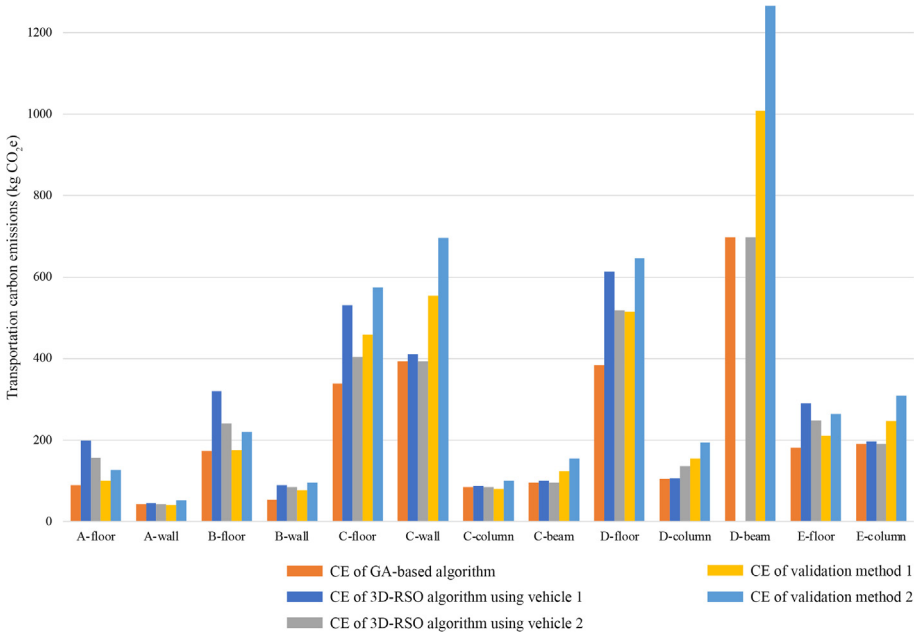

Fig. 10. Transportation CE of prefabricated elements in Projects A-E.

tasks. When vehicle 2 is adopted, the CE results are higher than 2.35 in three of five floor transportation tasks, two of three wall transportation tasks, and one of three column transportation tasks. The results are lower than 2.35 in other cases. Generally, the benchmark of 2.95 is higher than the results of all the other methods in most cases, as explained in Section 5.2 when the emission factor of 0.059 is higher than real-world emissions.

Looking into the average CE values, the trend is generally consistent with the task-specific data i.e., the result of the GA-based algorithm is the lowest among all results. The results of the 3D-RSO algorithm using vehicle 1 are higher than 2.35 and 2.95 in the transportation of prefabricated floors and are lower than those two benchmarks in the transportation of prefabricated walls, columns, and beams.

Regarding the difference across element types, the transportation CE of prefabricated floors is the highest, followed by that of prefabricated columns. The average CE of prefabricated walls is slightly higher than that of prefabricated beams. Meanwhile, the variance among the three BP algorithms is the largest in the transportation of prefabricated floor. This variance becomes smaller and remains similar in the transportation of the other three types of elements.

The difference in CE per unit prefabricated element can be explained by the difference in loading rate, as shown in Fig. 12, where the transportation CE per unit element decreases with the growth of the loading rate. Fig. 13 illustrates the loading rate of each transportation task. The GA-based algorithm obtains the highest average loading rate among all four element categories. The loading rate of the 3D-RSO algorithm using vehicle 2 ranks the second in prefabricated floors, walls, and beams and ranks the third in columns. This sequence is consistent with the sequence of the CE per unit element (i.e., a higher loading rate appears accompanied by a lower CE per unit element).

Besides, the average loading rate of elements varies with the element type, where the prefabricated floor has the lowest loading rate with the largest difference among the three algorithms. Prefabricated columns, however, have a smaller algorithm difference, while prefabricated walls and beams have the highest average loading rate.

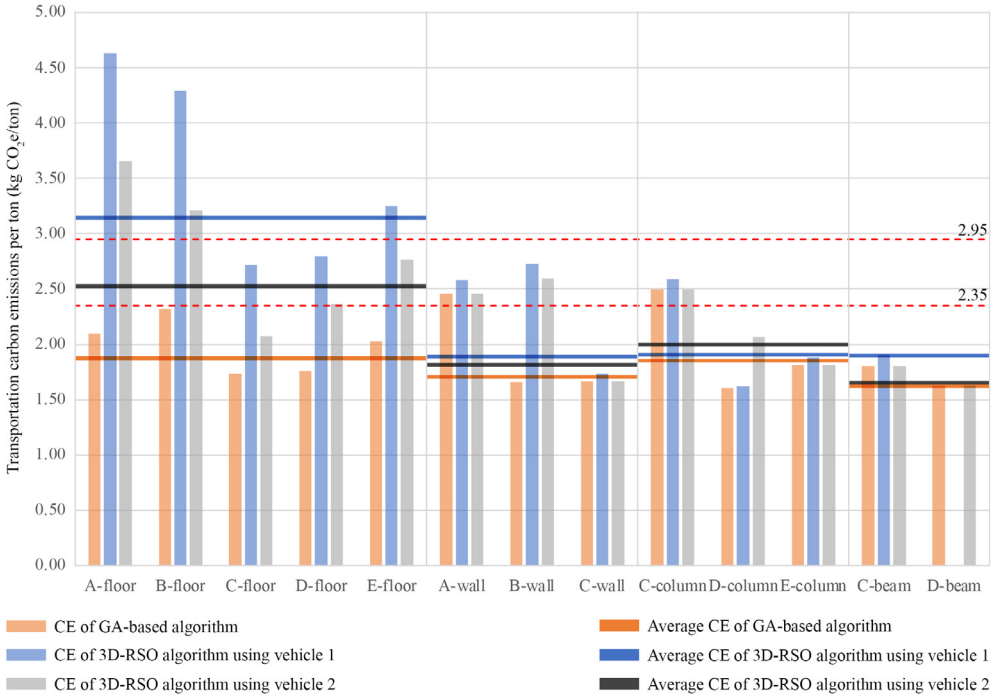

Fig. 11. Transportation CE per ton of different element types.

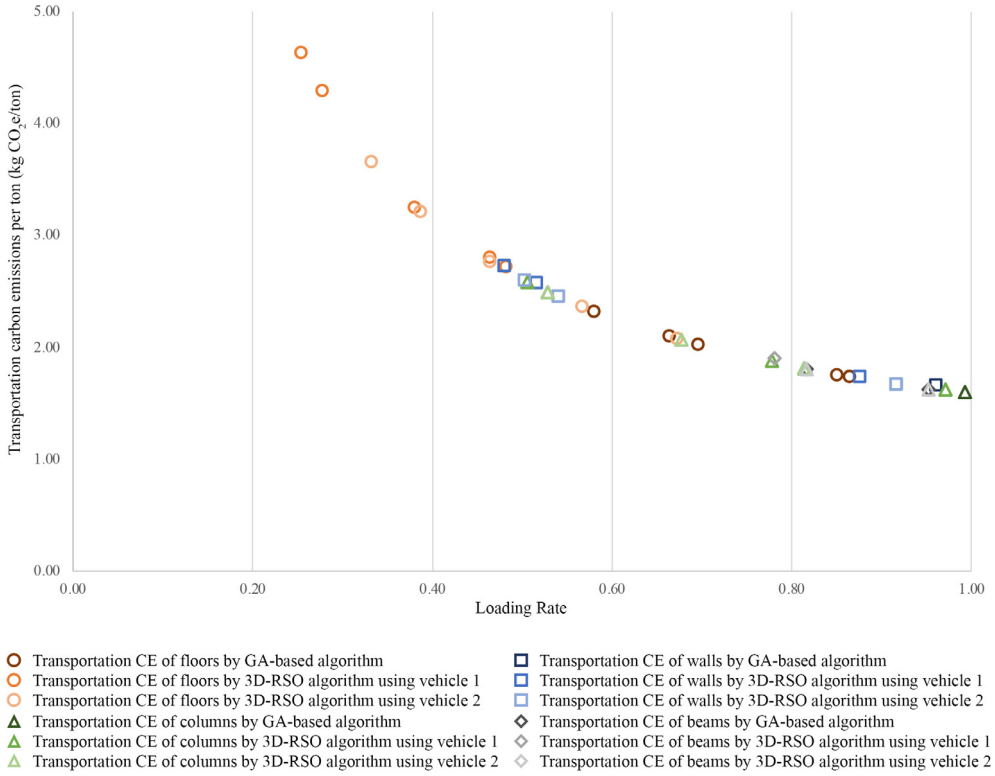

Fig. 12. The variation of CE of per ton elements with loading rate of vehicle.

5.4. Algorithm performance

This study employs a personal laptop to run all the algorithms; the laptop device specification includes an Intel Core i7-8665U CPU and 16 GB installed RAM. For an objective comparison among algorithms and projects, this study uses the identical parameter settings in the computing of each transportation task, as shown in Table 4.

Fig. 14 shows the solving process of the GA-based BP algorithm packing algorithm, in which the y-axis represents the value of the objective function (i.e., the CE per hour (kg CO_2e/h)), and the x-axis represents the generation in computing. The algorithm achieves

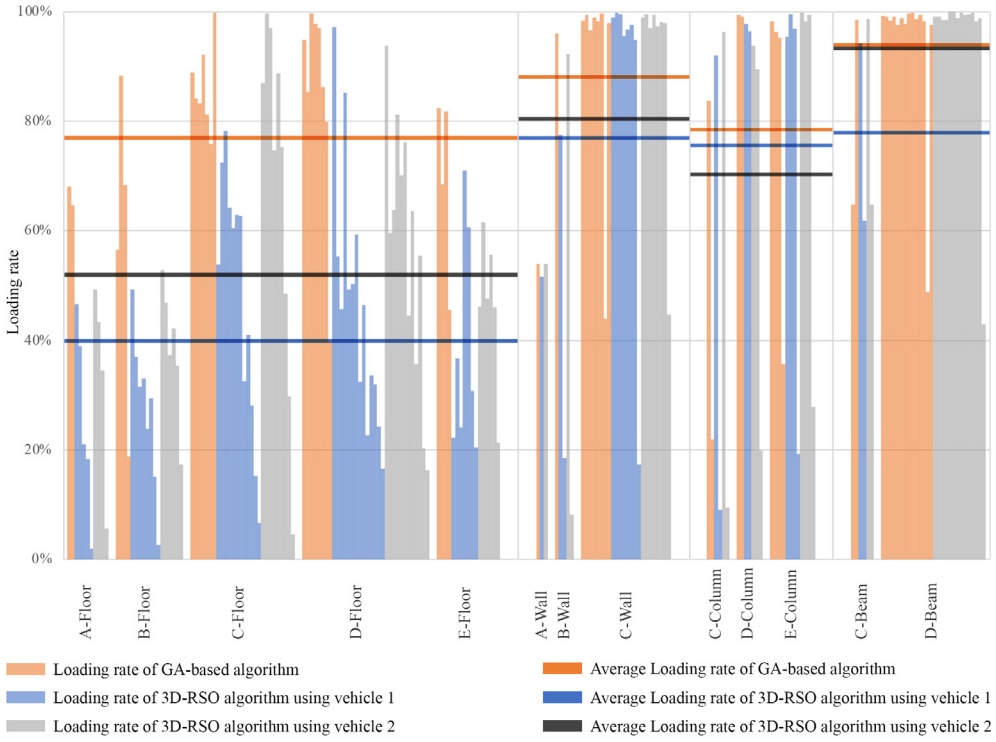

Fig. 13. Loading rate of different element types.

Table 4
Parameter setting of GA-based bin packing algorithm.

Parameter	Value
Population size	3, 200
Probability of performing crossover	0.7
Mutation operator F	0.5
Termination criteria	Generation = 1200

the lowest CE value within the first 600 generations in all 13 transportation tasks. Specifically, the optimum solutions are obtained within the first 50 generations in the transportation of prefabricated walls, columns, and beams, while the computing of prefabricated floors' transportation takes approximately 250 to 550 generations.

The average value in each generation is not a smooth curve in b-1 and d-3. Meanwhile, in a-1 and e-1, the average does not tend to the optimum value. This situation is because the objective function is not fully continuous. As shown in Eq. (41), the transportation CE is dominated by the number of vehicles, a discrete variable. Therefore, the average value may be stuck at a local-optimum value. This reason also explains the existence of fluctuations of optimal values in the figures a-1, b-1, b-2, d-1, and e-1.

Fig. 15 illustrates the computing time of the GA-based and 3D-RSO algorithms. The GA-based algorithm takes much more time than the 3D-RSO algorithms. Additionally, the total computing time and the computing time per piece element of the GA-based algorithm is growing with the total piece number increasing from 1880.13 s (10 pieces in C-column) to 85542.05 (168 pieces in C-floor) and from 188.01 s per piece (C-column) to 509.18 s per piece (C-floor), respectively. In contrast, the variation in total computing time of the 3D-RSO algorithm is not significant across all 13 transportation tasks, between 0.26 s and 0.35 s, leading to a negative relationship between the computing time per element piece and the number of prefabricated elements.

Fig. 16 illustrates the trade-off of computing time and CE when replacing the 3D-RSO algorithm with the GA-based algorithm, in which a closer distribution to the right bottom corner means a more efficient replacement and the opposite when a dot is approaching the left top corner. Generally, the replacement of 3D-RSO algorithm using vehicle 1 shows a more significant advantage than the 3D-RSO algorithm using vehicle 2 because of a larger CE reduction with a similar increase in computing time. Regarding the difference across element types, the CE reduction is more significant in the transportation of floors while less significant in the other three, especially in the transportation of columns and beams. This finding indicates that it is more efficient to employ the GA-based algorithm than the 3D-RSO algorithm in the transportation planning of prefabricated floors.

6. Discussion

In general, the BP-algorithm-based method provides a convincing output in the transportation CE calculation of prefabricated elements. As shown in Fig. 9, the calculation result of the BP-algorithm-based method is consistent with that of the Chinese official emission factor (Coe_i _1) [66] (validation method 1) at a 50 %-65 % loading rate. The variance between these two methods becomes significant with the loading rate shifting this range. According to Eq. (47), the CE result from the validation method 1 is linearly related to the weight of elements but without an original emission value (i.e., the interception is 0 in Fig. 9). This pattern indicates that the validation method 1 evenly distributes the CE generated by the vehicles themselves to each unit of prefabricated elements. The validation method 1 is suitable for estimating CE at a macro level (e.g., calculating the transportation CE of a city by multiplying the emission factor and cargo throughout) [67]. It is not, however, reasonable (accurate) in the micro-level application, especially when the loading rate is extremely low or high. In contrast, by considering the CE of vehicles, the BP-algorithm-based

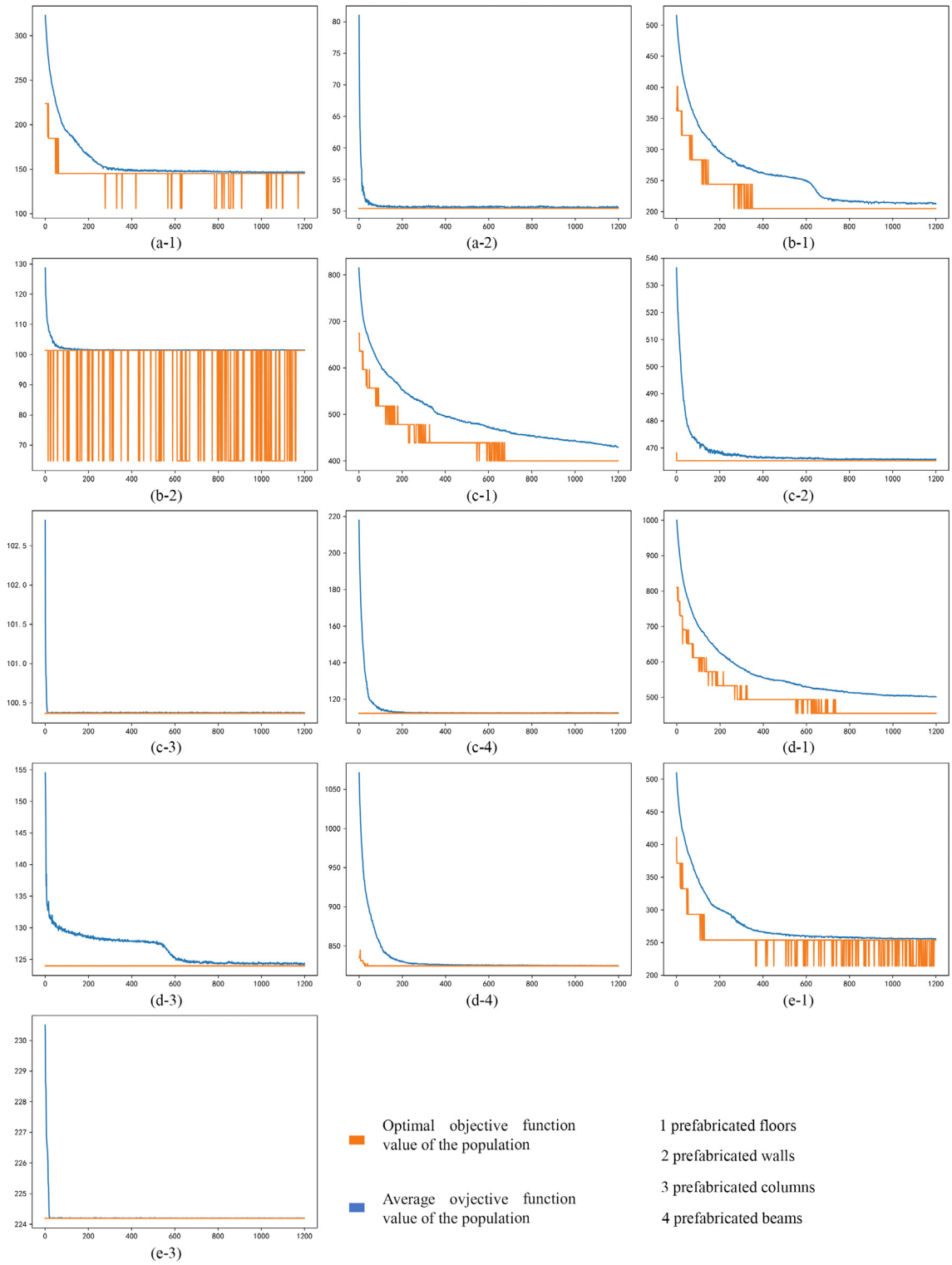

Fig. 14. Objective function value variation with the generation (x-axis is the value of objective function and y-axis is the number of generations).

method provides a more stable performance across different loading rates, making it more suitable for micro-level CE calculations.

The difference in basic calculation equations is reflected in the transportation CE results of five sample buildings. Fig. 10 and 11 illustrate the significant variance among the results of different calculation methods. The analysis of the loading rate provides a possible explanation for this difference. As shown in Fig. 12, the carbon emission per unit of elements decreases with the growth in loading rate. The validation methods 1 and 2 have a fixed loading rate, and thus the results for those methods are similar to the results of BP algorithms only when the loading rate is similar (between 50 % and 60 %), supporting the point above that the identical emission factor may not remain accurate in all situations. Therefore, results from the calculations based on the identical emission factors [6,27] need further validation on the actual loading rate, even those considering the actual transportation plan [29,30]

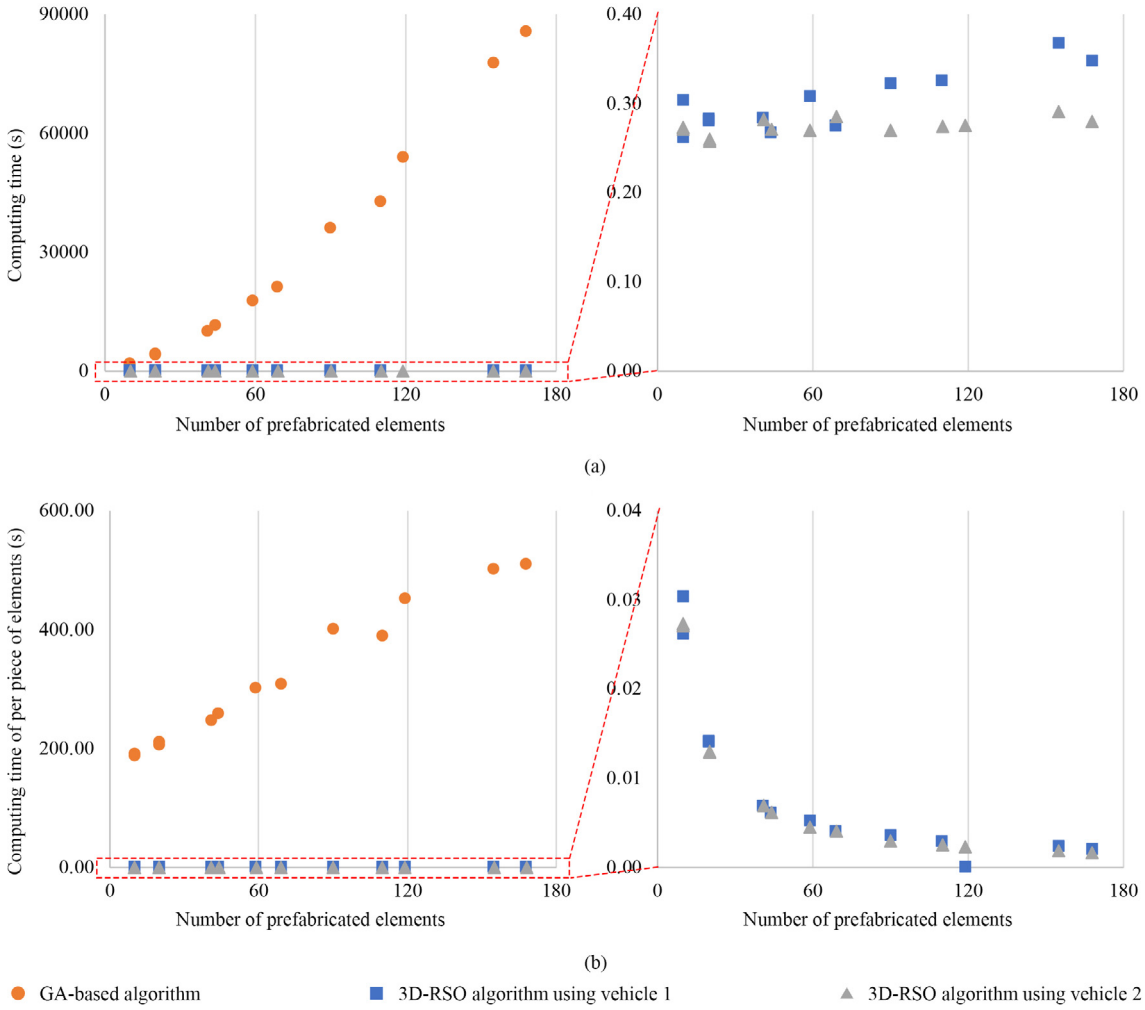

Fig. 15. Variation of the total computing time with the number of prefabricated elements (a) and Variation of the computing time per element piece with the number of prefabricated elements (b).

(because they employed an identical emission factor in the CE calculation of each vehicle).

Considering the relationship illustrated in Fig. 12, a possible solution towards more accurate CE results using the emission factor method is to provide different emission factors according to different loading rates and then select the corresponding factor in different transportation scenarios. Another potential method to refine the emission factor is providing different emission factors for different element types. Fig. 11 and 13 illustrate that there are significant differences in the average loading rate and CE per unit elements across different element types. Specifically, prefabricated floors have the lowest loading rate and thus the highest CE per unit elements. Prefabricated beams then have the second highest CE per unit elements. The loading rates of prefabricated walls and columns are similar and highest among all four categories. Although only precast concrete elements are studied in the current research, this relationship indicates the feasibility of providing element-type-specific emission factors. Such factors would be more convenient to implement in a general CE estimation because calculations based on emission factors saves time for bin packing problem modelling and solving.

This study employs two algorithms to search for the solutions to BP problems. In the case study on all five projects (13 transportation tasks in total), the GA-based algorithm employs the lowest number of vehicles, thus achieving the highest loading rate (Fig. 8 and 13). Considering the negative relationship between the carbon emission per unit of elements and the loading rate (Fig. 12), the GA-based algorithm has the lowest CE per unit of elements (Fig. 11), implying that the GA-based algorithm could provide more sustainable transportation plans than the 3D-RSO algorithm. Although the GA-based algorithm takes the longest time to obtain the result (as shown in Fig. 15), it is reasonable to apply this algorithm for a better solution, given that the average time spent on project sustainability analysis lasts 24 to 34 h [75].

Fig. 16 illustrates that the CE reduction caused by replacing the 3D-RSO algorithm with the GA-based algorithm is most obvious in the transportation of prefabricated floors and less significant in the other three categories. This variance suggests that the advantages of the GA-based algorithm (increasing the loading rate, thus reducing the CE) are less significant in some element types, and thus the disadvantage of a long computing period becomes more significant. Therefore, it is more reasonable to employ the 3D-RSO algorithm rather than the GA-based algorithm in these tasks for rapid computing without sacrificing significant performance.

Fig. 8 and 13 also illustrate that the differences in the vehicle number and the loading rate between the GA-based algorithm and the 3D-RSO algorithm increase with the growth in the number of prefabricated elements because this study employs an off-line packing mode. In this mode, a greater number of prefabricated elements provide algorithms with a larger solution space to explore

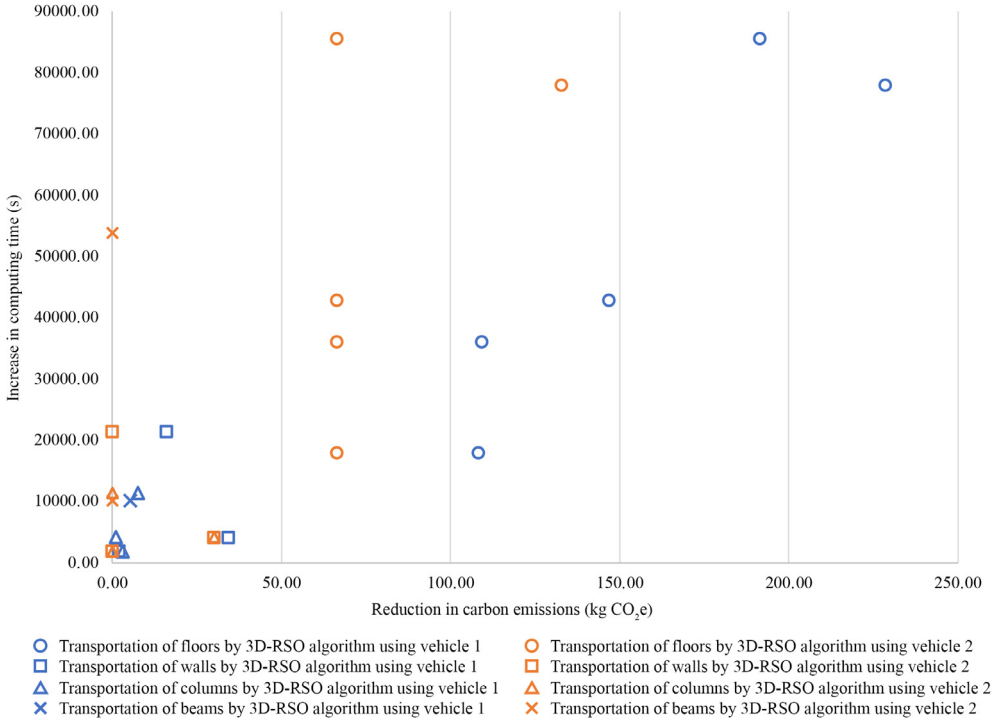

Fig. 16. Variation of the increase in computing time with the reduction in total carbon emissions.

the suitable element that fits the residual space, thus reducing the space waste and reducing the total number of vehicles. This effect therefore magnifies the performance difference between algorithms. Meanwhile, the accumulation of performance differences also grows with the element quantity and could lead to significant variance in the end—for example, the GA-based algorithm requires 33 %-50 % fewer vehicles than the 3D-RSO algorithm in the transportation of prefabricated floors in Project D (119 pieces) but the same number of vehicles in the transportation of prefabricated walls in Project A (10 pieces).

Considering that a higher loading rate leads to a lower transportation CE per unit of prefabricated elements (Fig. 12), the trend mentioned in the previous paragraph provides a potential method to reduce the transportation CE of prefabricated elements by considering a larger number of elements in one transportation batch. However, notably, the element quantity in one transportation batch is mainly affected by the storage capacity of the construction site and manufacturing factory, the manufacturing ability of the factory, and the construction plan [20,76]. Therefore, this potential method requires comprehensively optimising the whole construction process.

The findings signify the importance of considering real-world constraints in the transportation CE calculation of prefabricated elements. Compared with the calculation based on identical emission factors, the integration of the bin packing algorithm and modal model provides a more reliable result at the micro level, so the method is more suitable for CE prediction of single projects. This study ultimately provides a general model of prefabricated elements' transportation status using the classical bin packing problem, which caters to most prefabrication types. Meanwhile, the method allows for customised element sets, transportation constraints, transportation routine, and vehicle type. Architects and civil engineers can therefore employ the method to obtain project-specific transportation CE values according to specific local conditions, which could advance reliable project life-cycle sustainability analysis.

Additionally, the BP algorithm provides contractors with a detailed packing solution via the variable set of each element b_i. Contractors can use these variables to guide transportation planning, thus achieving the smallest vehicle number. Since the transportation cost is positively related to the vehicle number, the BP algorithm could also cause a reduction in transportation costs and construction fees.

This research adopts element size, element quantity, and vehicle type as variables in transportation CE calculation, by which CE analysis is quantitatively linked to architecture design and construction organisation. These relationships quantify the impacts of decisions at these two stages on CE, thus highlighting the opportunities to reduce CE by optimising prefabricated element division and construction planning. Scholars could adopt these variables in sustainability studies to obtain other practical CE optimisation methods apart from material replacement, factory selection, and fuel change—for example, for selecting prefabricated element types, limiting maximum element dimensions, and choosing the suitable vehicle size.

Despite the above contributions, this study also yields some limitations. The first is that the transportation modelling is not entirely accurate. The rotation resistance and vehicle acceleration are not considered in STP calculation. Regarding road conditions, the road slope is estimated from macro-level maps, which may not be fully consistent with the real-world condition. A field experiment could provide more reliable information. Secondly, the results of the GA-based algorithm are not necessarily the global optimum due to the inherent characteristic. The computing efficiency is not optimised because this study focuses on CE calculation and algorithm application rather than algorithm optimisation. However, the algorithm proposed provides suitable solutions to transportation CE calculation. Future works are encouraged to explore more efficient algorithms, achieve more accurate CE calculations, and integrate design optimisation via building information modelling (BIM) in the analysis.

7. Conclusions

Transportation of prefabricated elements generates significant CE during the whole lifecycle of prefabricated projects. However, existing calculation methods for transportation CE are not reliable at the micro level. This study therefore provides a transportation CE calculation method for prefabricated construction by integrating the bin packing problem and modal CE analysis model. Through the application in five study cases, the method has been shown to be reliable at either loading rate. Thus, it can be suitably applied in micro-level transportation CE calculation and prediction.

This research contributes to the environmental analysis of prefabricated construction. Although only five sample buildings are investigated, the result shows a non-negligible variance between the results from the BP-algorithm-based method and the conventional emission-factor method, suggesting the necessity to re-examine previous conclusions that transportation contributes to a small part of embodied carbon emissions in prefabricated construction. Architects and engineers could employ the BP-algorithm-based method to obtain project-specific transportation CE in the analysis of their projects for more reliable results. The detailed transportation plan provided by the BP algorithm ensures the feasibility of employing such a method in real-world practice. Additionally, this research contributes to the CE optimisation during the construction process. The variables used in the calculation relate element parameters to their environmental performances, providing opportunities to reduce CE through optimising the design of prefabricated elements and the construction plan. This optimisation method may be particularly useful in the technical design stage, providing more sustainable design alternatives that cause minor impacts on the architecture design. The government could implement this method as well during the drawing review to advance sustainable project design. Future works are expected to provide a more accurate and efficient CE calculation and integrate design optimisation in the analysis.

Data availability

The data and code can be shared if needed.

Declaration of Competing Interest

The authors declare that they have no known competing financial interests or personal relationships that could have appeared to influence the work reported in this paper.

Appendices A–C. Supplementary data

Supplementary data to this article can be found online at https://doi.org/10.1016/j.enbuild.2022.112640.

References

[1] BP, Statistical Review of World Energy 2021, 2021.
[2] United Nations Environment Programme, 2020 Global Status Report for Buildings and Construction: Towards a Zero-emission, 2021.
[3] M.K. Dixit, Life cycle recurrent embodied energy calculation of buildings: a review, J. Clean. Prod. 209 (2019) 731–754, https://doi.org/10.1016/j.jclepro.2018.10.230.
[4] M. Roberts, S. Allen, D. Coley, Life cycle assessment in the building design process – A systematic literature review, Build. Environ. 185 (2020), https://doi.org/10.1016/j.buildenv.2020.107274.
[5] L.F. Cabeza, L. Rincón, V. Vilariño, G. Pérez, A. Castell, Life cycle assessment (LCA) and life cycle energy analysis (LCEA) of buildings and the building sector: a review, Renew. Sustain. Energy Rev. 29 (2014) 394–416, https://doi.org/10.1016/j.rser.2013.08.037.
[6] J.L. Hao, B. Cheng, W. Lu, J. Xu, J. Wang, W. Bu, Z. Guo, Carbon emission reduction in prefabrication construction during materialization stage: A BIM-based life-cycle assessment approach, Sci. Total Environ. 723 (2020), https://doi.org/10.1016/j.scitotenv.2020.137870.
[7] Z. Yuan, C. Sun, Y. Wang, Design for manufacture and assembly-oriented parametric design of prefabricated buildings, Autom. Constr. 88 (2018) 13–22, https://doi.org/10.1016/j.autcon.2017.12.021.
[8] Z. Li, G.Q. Shen, X. Xue, Critical review of the research on the management of prefabricated construction, Habitat Int. 43 (2014) 240–249, https://doi.org/10.1016/j.habitatint.2014.04.001.
[9] C. Mao, Q. Shen, L. Shen, L. Tang, Comparative study of greenhouse gas emissions between off-site prefabrication and conventional construction methods: two case studies of residential projects, Energy Build. 66 (2013) 165–176.
[10] J. Hong, G.Q. Shen, C. Mao, Z. Li, K. Li, Life-cycle energy analysis of prefabricated building components: An input-output-based hybrid model, J. Clean. Prod. 112 (2016) 2198–2207, https://doi.org/10.1016/j.jclepro.2015.10.030.
[11] Y. Gao, Z. Li, H. Zhang, B. Yu, J. Wang, A carbon emission analysis model for prefabricated construction based on LCA, J. Eng. Manag. 32 (2018) 30–33. 10.13991/j.cnki.jem.2018.02.006.
[12] X. Cao, X. Li, Y. Zhu, Z. Zhang, A comparative study of environmental performance between prefabricated and traditional residential buildings in China, J. Clean. Prod. 109 (2015) 131–143, https://doi.org/10.1016/j.jclepro.2015.04.120.
[13] Y. Teng, K. Li, W. Pan, T. Ng, Reducing building life cycle carbon emissions through prefabrication: evidence from and gaps in empirical studies, Build. Environ. 132 (2018) 125–136, https://doi.org/10.1016/j.buildenv.2018.01.026.
[14] N. Sebaibi, M. Boutouil, Reducing energy consumption of prefabricated building elements and lowering the environmental impact of concrete, Eng. Struct. 213 (2020), https://doi.org/10.1016/j.engstruct.2020.110594.
[15] H. Wang, H. Zhang, K. Hou, G. Yao, Carbon emissions factor evaluation for assembled building during prefabricated component transportation phase, Energy Explor. Exploit. 39 (2021) 385–408, https://doi.org/10.1177/0144598720973371.
[16] A.F. Abd Rashid, S. Yusoff, A review of life cycle assessment method for building industry, Renew. Sustain. Energy Rev. 45 (2015) 244–248, https://doi.org/10.1016/j.rser.2015.01.043.
[17] Q. Du, T. Bao, Y. Li, Y. Huang, L. Shao, Impact of prefabrication technology on the cradle-to-site CO2 emissions of residential buildings, Clean Technol. Environ. Policy 21 (2019) 1499–1514, https://doi.org/10.1007/s10098-019-01723-y.
[18] C.K. Chau, T.M. Leung, W.Y. Ng, A review on life cycle assessment, life cycle energy assessment and life cycle carbon emissions assessment on buildings, Appl. Energy. 143 (2015) 395–413, https://doi.org/10.1016/j.apenergy.2015.01.023.
[19] A.E. Fenner, M. Razkenari, H. Hakim, C. Kibert, A Review of Prefabrication Benefits for Sustainable and Resilient Coastal Areas, 2017.
[20] B. Anvari, P. Angeloudis, W.Y. Ochieng, A multi-objective GA-based optimisation for holistic Manufacturing, transportation and Assembly of precast construction, Autom. Constr. 71 (2016) 226–241, https://doi.org/10.1016/j.autcon.2016.08.007.
[21] F. Wong, Y.T. Tang, Comparative embodied carbon analysis of the prefabrication elements compared with in-situ elements in residential building development of Hong Kong, World Acad. Sci. Eng. Technol. 62 (2012) 161–166.
[22] Y.H. Dong, L. Jaillon, P. Chu, C.S. Poon, Comparing carbon emissions of precast and cast-in-situ construction methods – A case study of high-rise private building, Constr. Build. Mater. 99 (2015) 39–53, https://doi.org/10.1016/j.conbuildmat.2015.08.145.
[23] M.K. Dixit, Life cycle embodied energy analysis of residential buildings: A review of literature to investigate embodied energy parameters, Renew. Sustain. Energy Rev. 79 (2017) 390–413, https://doi.org/10.1016/j.rser.2017.05.051.
[24] P. Chastas, T. Theodosiou, D. Bikas, Embodied energy in residential buildings-towards the nearly zero energy building: a literature review, Build. Environ. 105 (2016) 267–282, https://doi.org/10.1016/j.buildenv.2016.05.040.
[25] D. Li, P. Cui, Y. Lu, Development of an automated estimator of life-cycle carbon emissions for residential buildings: a case study in Nanjing, China, Habitat Int. 57 (2016) 154–163, https://doi.org/10.1016/j.habitatint.2016.07.003.
[26] T. Jafary Nasab, S.M. Monavari, S.A. Jozi, H. Majedi, Assessment of carbon footprint in the construction phase of high-rise constructions in Tehran, Int. J. Environ. Sci. Technol. 17 (2020) 3153–3164, https://doi.org/10.1007/s13762-019-02557-3.
[27] S.T. Abey, K.B. Anand, Embodied energy comparison of prefabricated and conventional building construction, J. Inst. Eng. Ser. A. 100 (2019) 777–790, https://doi.org/10.1007/s40030-019-00394-8.
[28] China Institute of Building Standard Design & Research, Drawing Collection for National Building Standard Design, (2015).
[29] G. Liu, R. Chen, P. Xu, Y. Fu, C. Mao, J. Hong, Real-time carbon emission monitoring in prefabricated construction, Autom. Constr. 110 (2020), https://doi.org/10.1016/j.autcon.2019.102945.
[30] G. Liu, H. Yang, Y. Fu, C. Mao, P. Xu, J. Hong, R. Li, Cyber-physical system-based real-time monitoring and visualization of greenhouse gas emissions of prefabricated construction, J. Clean. Prod. 246 (2020), https://doi.org/10.1016/j.jclepro.2019.119059.
[31] Y. Chen, Y. Zhu, Models for life-cycle enegy consumption and environmental emissions in residential buildings, J. Tsinghua Univeris. (Sci. Technol.) 50 (2010) 5.

[32] R. Tu, T. Li, C. Meng, J. Chen, Z. Sheng, Y. Xie, F. Xie, F. Yang, H. Chen, Y. Li, J. Gao, Y. Liu, Real-world emissions of construction mobile machines and comparison to a non-road emission model, Sci. Total Environ. 771 (2021), https://doi.org/10.1016/j.scitotenv.2021.145365.
[33] A. Wang, R. Tu, J. Xu, Z. Zhai, M. Hatzopoulou, A novel modal emission modelling approach and its application with on-road emission measurements, Appl. Energy 306 (2022), https://doi.org/10.1016/j.apenergy.2021.117967.
[34] U.S.E.P.A. EPA, Exhaust Emission Rates for Light-Duty Onroad Vehicles in MOVES3, 2020.
[35] H.W. Wallace, B.T. Jobson, M.H. Erickson, J.K. McCoskey, T.M. VanReken, B.K. Lamb, J.K. Vaughan, R.J. Hardy, J.L. Cole, S.M. Strachan, W. Zhang, Comparison of wintertime CO to NO x ratios to MOVES and MOBILE6.2 on-road emissions inventories, Atmos. Environ. 63 (2012) 289–297, https://doi.org/10.1016/j.atmosenv.2012.08.062.
[36] S. Vallamsundar, J. Lin, MOVES Versus MOBILE: Comparison of greenhouse gas and criterion pollutant emissions, Transp. Res. Rec. (2011) 27–35, https://doi.org/10.3141/2233-04.
[37] E.M. Fujita, D.E. Campbell, B. Zielinska, J.C. Chow, C.E. Lindhjem, A. DenBleyker, G.A. Bishop, B.G. Schuchmann, D.H. Stedman, D.R. Lawson, Comparison of the MOVES2010a, MOBILE6.2, and EMFAC2007 mobile source emission models with on-road traffic tunnel and remote sensing measurements, J. Air Waste Manage. Assoc. 62 (2012) 1134–1149, https://doi.org/10.1080/10962247.2012.699016.
[38] L. Zhang, X. Hu, R. Qiu, A review of research on emission models of vehicle exhausts, World Sci. Technol. R&D 39 (2017) 355–362.
[39] X. Shen, T. Lv, X. Zhang, X. Cao, X. Li, B. Wu, X. Yao, Y. Shi, Q. Zhou, X. Chen, Z. Yao, Real-world emission characteristics of black carbon emitted by on-road China IV and China V diesel trucks, Sci. Total Environ. 799 (2021), https://doi.org/10.1016/j.scitotenv.2021.149435.
[40] J.W. Chung, B.H. LEE, S.S. Lee, D.J. Kim, J.Y. Park, Y.M. Goo, STUDY ON ANALYSIS OF REAL ROAD DRIVING CHARACTERISTICS OF HEAVY-DUTY GAS DELIVERY TRACTOR, Int. J. Automot. Technol. 13 (2012) 293–300. 10.1007/s12239
[41] J. Wang, H. Gui, Z. Yang, T. Yu, X. Zhang, J. Liu, Real-world gaseous emission characteristics of natural gas heavy-duty sanitation trucks, J. Environ. Sci. (China) 115 (2022) 319–329, https://doi.org/10.1016/j.jes.2021.06.023.
[42] C.D. Desouza, D.J. Marsh, S.D. Beevers, N. Molden, D.C. Green, Real-world emissions from non-road mobile machinery in London, Atmos. Environ. 223 (2020), https://doi.org/10.1016/j.atmosenv.2020.117301.
[43] B. Muresan, A. Capony, M. Goriaux, D. Pillot, P. Higelin, C. Proust, A. Jullien, Key factors controlling the real exhaust emissions from earthwork machines, Transp. Res. Part D Transp. Environ. 41 (2015) 271–287, https://doi.org/10.1016/j.trd.2015.10.002.
[44] J. Seo, B. Yun, J. Kim, M. Shin, S. Park, Development of a cold-start emission model for diesel vehicles using an artificial neural network trained with real-world driving data, Sci. Total Environ. 806 (2022), https://doi.org/10.1016/j.scitotenv.2021.151347.
[45] E.G. Coffman, J. Csirik, G. Galambos, S. Martello, D. Vigo, P.M. Pardalos, D.Z. Du, R.L. Graham, Bin packing approximation algorithms: Survey and classification, in: Handb. Comb. Optim., 2013: pp. 455–531. 10.1007/978-1-4419-7997-1_35.
[46] H. Solomon, H. Weiner, A review of the packing problem, Commun. Stat. - Theory Methods 15 (1986) 2571–2607, https://doi.org/10.1080/03610928608829274.
[47] N.G. Hall, S. Ghosh, R.D. Kankey, S. Narasimhan, W.S.T. Rhee, Bin packing problems in one dimension: Heuristic solutions and confidence intervals, Comput. Oper. Res. 15 (1988) 171–177, https://doi.org/10.1016/0305-0548(88)90009-3.
[48] A. Lodi, S. Martello, M. Monaci, Two-dimensional packing problems: a survey, Eur. J. Oper. Res. 141 (2002) 241–252, https://doi.org/10.1016/S0377-2217(02)00123-6.
[49] O. Faroe, D. Pisinger, M. Zachariasen, Guided local search for the three-dimensional bin-packing problem, INFORMS J. Comput. 15 (2003) 267–283, https://doi.org/10.1287/ijoc.15.3.267.16080.
[50] A. Lodi, S. Martello, D. Vigo, Heuristic algorithms for the three-dimensional bin packing problem, Eur. J. Oper. Res. 141 (2002) 410–420, https://doi.org/10.1016/S0377-2217(02)00134-0.
[51] C. Munien, A.E. Ezugwu, Metaheuristic algorithms for one-dimensional bin-packing problems: A survey of recent advances and applications, J. Intell. Syst. 30 (2021) 636–663, https://doi.org/10.1515/jisys-2020-0117.
[52] Z. Shang, J. Gu, Q. Huang, Algorithm and application of packing problem, 1st ed., China University of Mining and Technology Assets Management CO., LTD., Xuzhou City, 2020.
[53] A. Lim, B. Rodrigues, Y. Yang, 3-D container packing heuristics, Appl. Intell. 22 (2005) 125–134, https://doi.org/10.1007/s10489-005-5601-0.
[54] M.M. Baldi, T.G. Crainic, G. Perboli, R. Tadei, The generalized bin packing problem, Transp. Res. Part E Logist. Transp. Rev. 48 (2012) 1205–1220, https://doi.org/10.1016/j.tre.2012.06.005.
[55] I. Moon, T.V.L. Nguyen, Container packing problem with balance constraints, OR Spectr. 36 (2014) 837–878, https://doi.org/10.1007/s00291-013-0356-1.
[56] S. Erbayrak, V. Özkır, U. Mahir Yıldırım, Multi-objective 3D bin packing problem with load balance and product family concerns, Comput. Ind. Eng. 159 (2021), https://doi.org/10.1016/j.cie.2021.107518.
[57] L. Cruz Reyes, D.M. Nieto-Yáñez, N. Rangel-Valdez, J.A. Herrera Ortiz, J. González B, G. Castilla Valdez, J.F. Delgado-Orta, DiPro: An Algorithm for the Packing in Product Transportation Problems with Multiple Loading and Routing Variants BT - MICAI 2007: Advances in Artificial Intelligence, in: A. Gelbukh, Á.F. Kuri Morales (Eds.), Springer Berlin Heidelberg, Berlin, Heidelberg, 2007: pp. 1078–1088
[58] Q. Liu, H. Cheng, T. Tian, Y. Wang, J. Leng, R. Zhao, H. Zhang, L. Wei, Algorithms for the variable-sized bin packing problem with time windows, Comput. Ind. Eng. 155 (2021), https://doi.org/10.1016/j.cie.2021.107175.
[59] R.R. Amossen, D. Pisinger, Multi-dimensional bin packing problems with guillotine constraints, Comput. Oper. Res. 37 (2010) 1999–2006, https://doi.org/10.1016/j.cor.2010.01.017.
[60] B.S. Baker, E.G. Coffman, R.L. Rivest, Orthogonal Packings in Two Dimensions., Proc. - Annu. Allert. Conf. Commun. Control. Comput. 9 (1978) 626–635. 10.1137/0209064.
[61] U.S.E.P.A. EPA, Overview of EPA ' s MOtor Vehicle Emission Simulator (MOVES3), 2020.
[62] U.S.E.P.A. EPA, Exhaust Emission Rates for Heavy-Duty Onroad Vehicles in MOVES3, 2020.
[63] Y. Yue, G. Song, G. Huang, L. Yu, Application of MOVES in the microscopic evaluation of traffic emissions, J. Transp. Inf. Saf. 31 (2013) 47–53.
[64] G. Huang, G. Song, L. Yu, Y. Xu, Overview of the comprehensive mobile source emissions model: MOVES, Comput. Commun. 28 (2010) 49–53.
[65] Geatpy team, Geatpy, (2022). http://geatpy.com (accessed 13 April 2022).
[66] CCG, China Products Carbon Footprint Factors Database, (2022). http://lca.cityghg.com.
[67] C. Lü, Z. Zhang, X. Chen, D. Ma, B. Cai, Study on CO2 emission factors of road transport in Chinese provinces, China, Environ. Sci. 41 (2021) 3122–3130.
[68] Mohurd, Calculation Standard of Building Carbon Emissions, People's Republic of China, 2014.
[69] School of Transporation and Logistics of Southwest Jiaotong University, Preliminary Report on the Freight Industry, 2020.
[70] O. Delgado, H. Li, Market Analysis and Fuel Efficiency Technology Potential of Heavy-Duty Vehicles in China, 2017.
[71] China Automotive Technology and Research Center, China Green Freight Assessment, Bejing Oper. (2018).
[72] Mohurd, Technical Specification for Precast Concrete Structures, People's Republic of China, 2014.
[73] Togpographic-map.com, Topographic map of China, (2022). https://zh-cn.topographic-map.com (accessed 21 March 2022).
[74] Google Maps, Map of China, (2022). https://www.google.com/maps (accessed 21 March 2022).
[75] T. Jusselme, E. Rey, M. Andersen, Surveying the environmental life-cycle performance assessments: practice and context at early building design stages, Sustain. Cities Soc. 52 (2020), https://doi.org/10.1016/j.scs.2019.101879.
[76] Z. Wang, H. Hu, J. Gong, Framework for modeling operational uncertainty to optimize offsite production scheduling of precast components, Autom. Constr. 86 (2018) 69–80, https://doi.org/10.1016/j.autcon.2017.10.026.